Moving Target Detection Using Colocated MIMO Radar on Multiple Distributed Moving Platforms

Peng Chen, *Member, IEEE*, Le Zheng, *Member, IEEE*, Xiaodong Wang, *Fellow, IEEE*, Hongbin Li, *Senior Member, IEEE*, and Lenan Wu

***Abstract*—In this paper, we consider the problem of moving target detection, and a novel radar system with multiple moving platforms is proposed. Each moving platform is equipped with multiple colocated antennas and serves as a transmitter or a receiver. Thus, this system possesses the advantages of both distributed and colocated multiple-input multiple-output radars. To exploit the clutter sparsity in the surveillance area, a novel compressed sensing (CS)-based model is proposed. Since the clutter cannot exactly reside on discretized grids often employed by most CS approaches, a novel two-step algorithm which extends the orthogonal matching pursuit is proposed to reconstruct the off-grid clutter. Then, a fusion center combines all received signals by using a generalized likelihood ratio test to detect the moving target. To further improve the detection performance, a novel online waveform optimization algorithm is developed to maximize the signal-to-clutter-and-noise ratios of each transmitter platform. Extensive simulation results are provided to demonstrate the effectiveness of the proposed radar system and algorithms.**

***Index Terms*—Moving target detection, multi-input multi-output (MIMO) radar, waveform optimization, moving radar platform, compressed sensing.**

I. Introduction

DIFFERENT from traditional array radars, independent waveforms are transmitted in multi-input multi-output (MIMO) radar systems. As a result, target detection, estimation and tracking performances can be improved by exploiting both the spatial and waveform diversities [1], [2]. Since a radar system on moving platforms provides more opportunities to approach and detect the target, extending the moving distributed MIMO radar concept of [3], in this paper, a novel radar system with multiple moving platforms is proposed, where colocated MIMO antennas are deployed in each platform. In such a radar system, the advantages of both colocated and distributed MIMO radars can be exploited, and waveforms can be optimized to improve the target detection performance.

In the target detection problem, the echo from the target is interfered by those from the radar clutter, which can be categorized into the following two types:

1) *Homogeneous clutter:* The clutter distributions are identical among the detection and adjacent areas, and the clutter information can be estimated from the secondary data of the adjacent areas [4]–[6];
2) *Non-homogeneous clutter:* The non-stationarity of the radar working environment can cause the non-homogeneity of clutter, where the clutter distributions are different among resolution cells and changing over time [3], [7].

During the process of target detection in homogeneous clutter, the clutter information is estimated from the adjacent areas without a target. For example, by estimating the covariance matrix of the clutter, the detector based on the generalized likelihood ratio test (GLRT) is proposed in [8], [9]. Moreover, by estimating the compound-Gaussian clutter, the GLRT for the moving target is proposed in [10].

However, with non-homogeneous clutter, the clutter distributions are location dependent and changing with time, which must be estimated from the detection area instead of the adjacent areas [11]. Different methods have been proposed for the purpose of clutter parameter estimation. For example, non-homogeneous clutter is described by Gaussian distributions with different means and variances in [12]. In distributed MIMO radar, random matrices [13], auto-regressive (AR) models [14] and low-rank subspaces [7] can be used to model non-homogeneous clutter. Given clutter parameter estimates, various detection methods, such as the GLRT [15] and the Rao-and-Wald detector [16], can be applied.

To further improve the target detection and estimation performance, the radar system can be optimized based on the characteristics of the target, clutter and noise. In MIMO radar, two types of optimization can be performed.

1) *Beampattern design:* The transmitted waveforms and weight vector are chosen to approach a desired spatial beampattern [17]–[21].
2) *Waveform optimization:* Since independent waveforms are transmitted in MIMO radar, the waveforms can be optimized to improve some specific performance metrics. For example, the mutual information between the

Manuscript received November 3, 2016; revised April 13, 2017; accepted June 5, 2017. Date of publication June 12, 2017; date of current version July 3, 2017. The associate editor coordinating the review of this manuscript and approving it for publication was Prof. Marco Lops. This work was supported in part by the National Natural Science Foundation of China under Grants 61271204 and 61601281, in part by the Fundamental Research Funds for the Central Universities, and in part by the U.S. National Science Foundation under Grant CIF1064575. *(Corresponding author: Le Zheng.)*

P. Chen is with the State Key Laboratory of Millimeter Waves, Southeast University, Nanjing 210096, China (e-mail: chenpengdsp@seu.edu.cn).

L. Zheng and X. Wang are with the Electrical Engineering Department, Columbia University, New York, NY 10027 USA (e-mail: le.zheng.cn@gmail.com; wangx@ee.columbia.edu).

H. Li is with the Department of Electrical and Computer Engineering, Stevens Institute of Technology, Hoboken, NJ 07030 USA (e-mail: Hongbin.Li@stevens.edu).

L. Wu is with the School of Information Science and Engineering, Southeast University, Nanjing 210096, China (e-mail: wuln@seu.edu.cn).

Color versions of one or more of the figures in this paper are available online at http://ieeexplore.ieee.org.

Digital Object Identifier 10.1109/TSP.2017.2714999

received waveform and the target impulse response is maximized in [22]. For the environment with both clutter and noise interferences, the waveforms can also be optimized to improve the target estimation and detection performances [23]–[25]. Additionally, the joint optimization of both the receiver filter and waveforms is proposed in [26]. Several other optimization methods, including the alternating projection-based method [27] and the ambiguity function-based method [28], [29], have also been proposed.

However, all these optimization methods are based on the estimated information from the secondary data in the adjacent areas, including the knowledge of the clutter and noise. When the clutter is non-homogeneous, such knowledge cannot be obtained from the secondary data, and must be estimated from the primary data in the detection area [12], [30], [31]. Therefore, in this paper, based on the estimated information of the target and clutter from the primary data, a novel method is proposed to optimize the transmitted waveforms online by maximizing the signal-to-clutter-and-noise ratios (SCNRs) of the received signals in multiple moving platforms with colocated MIMO antennas.

Since the radar platforms considered in this paper are moving and the clutter distributions are different among resolution cells, it is more appropriate to describe the clutter by a non-homogeneous model. In particular, by exploiting the sparsity of clutter a compressed sensing (CS)-based model is proposed to describe the clutter. When the clutter scatterers are on the discretized grids, the traditional CS methods including ℓ_1 relaxation algorithms or the greedy algorithms [32] can be adopted to reconstruct the sparse signal. On the other hand, when off-grid problem is considered and the clutter scatterers are not on the discretized grids, a joint CS problem can be formulated, and methods such as the JOMP algorithm [33] can be adopted to reconstruct the sparse vector. To further improve the CS reconstruction performance, we propose a novel two-step OMP algorithm, where the on-grid and off-grid components of the sparse vector are iteratively estimated using the dictionary matrix and the derivative matrix, respectively. Then, based on the estimated information about the target and clutter from the received signal, the GLRT is performed to detect the target.

The remainder of this paper is organized as follows. The MIMO radar model with colocated antennas on multiple moving platforms is given in Section II. The GLRT for detecting moving target is proposed in Section III. Section IV proposes the CS-based method to estimate the target and clutter parameters. Then, Section V optimizes the transmitted waveforms of each transmitter moving platform. Simulation results are given in Section VI. Finally, Section VII concludes the paper.

II. Colocated MIMO Radar System on Multiple Moving Platforms

Based on the distance between antennas, MIMO radar systems can be categorized into the following types:

1) *Distributed MIMO radar:* The antennas are widely separated, and the spatial diversity of the target's radar cross section (RCS) can be exploited to improve the target detection performance [34].

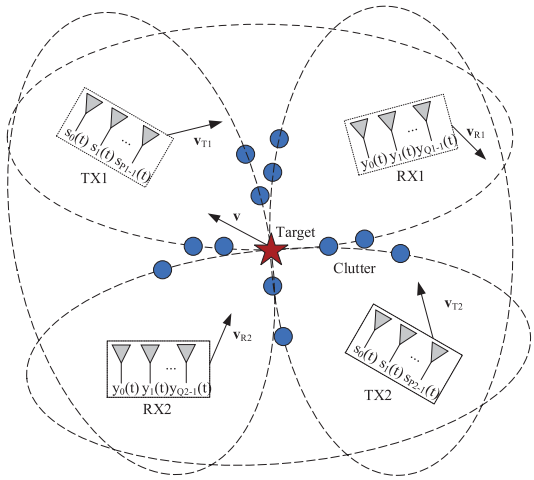

Fig. 1. Colocated MIMO radar system on multiple moving platforms.

2) *Colocated MIMO radar:* The antennas are close to each other, and adaptive array processing, including waveform and beam-pattern optimization [35], [36], can be performed to exploit the waveform diversity. Additionally, according to the position of transmitter platform (TX) and receiver platform (RX), colocated MIMO radar can be categorized into the following types:
   a) *Monostatic MIMO radar:* The TX and RX are close to each other, and all antennas are colocated. Then, more reliable target detection and beam-pattern design can be achieved [37].
   b) *Bistatic MIMO radar:* The TX and RX are widely separated, and the antennas are only colocated inside TX or RX. Then, the higher target localization performance can be achieved with the different view angles from TX and RX [37], [38].

Different from the existing distributed and colocated MIMO radar systems, Fig. 1 shows the proposed MIMO radar system, where multiple widely separated moving platforms are deployed and MIMO antennas are employed in each moving platform. More waveform diversity can be introduced, and the transmitted waveforms can be optimized to further improve the target detection performance. Therefore, the proposed system is able to offer some of the benefits of both colocated and distributed MIMO radar and provide a tradeoff between these two systems. Since TXs and RXs are widely separated, this radar system is also an extended version of the bistatic MIMO radar. There are multiple TX-RX pairs and both TX and RX are colocated radars, so collectively, this is a multi-static phased-array radar. Therefore, a fusion center is needed to collected all the data and process the signals together.

The numbers of TXs and RXs are M and N, respectively, and the numbers of antennas of the m-th TX $(0 \le m \le M-1)$ and the n-th RX $(0 \le n \le N-1)$ are P_m and Q_n, respectively. In each radar platform, the distance between the antennas is d_T, which is a half of the wavelength. The velocities of the m-th TX, the n-th RX and the target are $\boldsymbol{v}_{T,m} \in \mathbb{R}^2$, $\boldsymbol{v}_{R,n} \in \mathbb{R}^2$ and $\boldsymbol{v} \in \mathbb{R}^2$, respectively, where we assume that both $\boldsymbol{v}_{T,m}$ and $\boldsymbol{v}_{R,n}$ are known but not $\boldsymbol{v}$. $\boldsymbol{p} \in \mathbb{R}^2$, $\boldsymbol{p}_{T,m} \in \mathbb{R}^2$ and $\boldsymbol{p}_{R,n} \in \mathbb{R}^2$ denote the positions of target, the m-th TX and the n-th RX respectively.

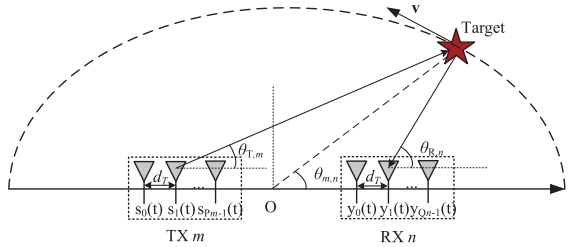

Fig. 2. The angle relationship between the moving target and radar platforms.

As shown in Fig. 1, the detection area for each TX-RX pair forms an ellipse, with the TX and RX being the focal points, and the echo waveform from the target is interfered by that from clutter in the same ellipse. Since the target and radar platforms are non-stationary and the geographic distributions of clutter are different among TX-RX pairs, the clutter interferences are non-homogeneous, and the clutter information can only be obtained from the detection area instead of the adjacent areas. Moreover, the Doppler frequencies of clutter are also nonzero because of the relative movement between radar platforms and clutter.

As shown in Fig. 2, the radar waveforms are transmitted by the m-th TX, echoed from the moving target and received by the n-th RX. We denote (m,p) as the p-th antenna of the m-th TX $(0 \le p \le P_m - 1)$, and (n,q) as the q-th antenna of the n-th RX $(0 \le q \le Q_n - 1)$. Then, the continuous-time transmitted waveform from the (m,p)-th TX antenna can be expressed as $\mathrm{Re}\left\{s_{m,p}(t)\, e^{j2\pi f_c t}\right\}$, where $s_{m,p}(t)$ denotes the baseband complex waveform, f_c denotes the carrier frequency, c denotes the velocity of light, and T denotes the pulse duration. K pulses are transmitted with the pulse repetition interval (PRI) being T_p. Assuming $MT \ll T_p$, the signals transmitted by different TXs are orthogonal. Then, the received signal by the (n,q)-th RX antenna during the k-th pulse $(0 \le k \le K-1)$ of the transmitted signal from the m-th TX is given by [3], [4]

$$y_{m,(n,q)}(t'_k) = \mathrm{Re}\left\{\sum_{p=0}^{P_m-1} \alpha_{m,n} s_{m,p}(t'_k)\, e^{j2\pi t'_k f'}\right\}, \quad (1)$$

where $f' \triangleq f_c + f_{d,m,n}(\theta_{m,n}, \boldsymbol{v})$, $t'_k \triangleq t - \tau_{(m,p),(n,q)}(\theta_{m,n}) - kT_p$ $(0 \le t'_k \le T_p)$, and $\alpha_{m,n}$ denotes the scattering coefficient of the target. The delay from the (m,p)-th TX antenna to the (n,q)-th RX antenna is defined as $\tau_{(m,p),(n,q)}(\theta_{m,n})$, which is a function of the target angle $\theta_{m,n}$. For simplicity, all delays are relative to the delay between the 0-th TX antenna and the 0-th RX antenna, i.e., $\tau_{(m,p),(n,q)}(\theta_{m,n}) \leftarrow \tau_{(m,p),(n,q)}(\theta_{m,n}) - \tau_{(m,0),(n,0)}(\theta_{m,n})$. Moreover, for the m-th TX and n-th RX, the relative movement between the target and radar platforms causes the Doppler frequency $f_{d,m,n}(\theta_{m,n}, \boldsymbol{v})$, which is a function of the target angle $\theta_{m,n}$ and velocity $\boldsymbol{v}$. Since the velocities of TXs and RXs are known, we omit $\boldsymbol{v}_{T,m}$ and $\boldsymbol{v}_{R,n}$ in $f_{d,m,n}(\theta_{m,n}, \boldsymbol{v})$. The expressions of $\tau_{(m,p),(n,q)}(\theta_{m,n})$ and $f_{d,m,n}(\theta_{m,n}, \boldsymbol{v})$, and the target view angle $\theta_{T,m}$ from the m-th TX and the target view angle $\theta_{R,n}$ from the n-th RX are all given in Appendix.

For the convenience of analysis, a vector $\boldsymbol{s}_{m,p} \in \mathbb{C}^{L\times 1}$ is used to represent the transmitted waveform $s_{m,p}(t)$, where L denotes the length of the signal vector sampled from the transmitted waveform $s_{m,p}(t)$. Then, after down conversion, the discrete form of the received signal in (1) during the k-th pulse can be rewritten as (2) shown at the bottom of this page, where $\boldsymbol{S}_m \triangleq [\boldsymbol{s}_{m,0}, \boldsymbol{s}_{m,1}, \ldots, \boldsymbol{s}_{m,P_m-1}]$ denotes the waveform matrix for the m-th TX, and more details about the sampling processes are given at the end of Appendix. $a_{m,p}(\theta_{m,n})$ and $b_{n,q}(\theta_{m,n})$ denote as the p-th and q-th entries of the steering vectors $\boldsymbol{a}_m(\theta_{m,n})$ and $\boldsymbol{b}_n(\theta_{m,n})$, respectively, and

$$\boldsymbol{a}_m(\theta_{m,n}) \triangleq \left[1, e^{-j2\pi \frac{f_c}{c} d_T \cos\theta_{T,m}}, \ldots, e^{-j2\pi \frac{f_c}{c}(P_m-1) d_T \cos\theta_{T,m}}\right]^T, \quad (3)$$

$$\boldsymbol{b}_n(\theta_{m,n}) \triangleq \left[1, e^{-j2\pi \frac{f_c}{c} d_T \cos\theta_{R,n}}, \ldots, e^{-j2\pi \frac{f_c}{c}(Q_n-1) d_T \cos\theta_{R,n}}\right]^T. \quad (4)$$

For K pulses, the Doppler vector of the m-th TX and the n-th RX can be obtained as

$$\boldsymbol{d}(f_{d,m,n}(\theta_{m,n}, \boldsymbol{v})) = \left[1, e^{j2\pi f_{d,m,n}(\theta_{m,n},\boldsymbol{v})T_p}, \ldots, e^{j2\pi f_{d,m,n}(\theta_{m,n},\boldsymbol{v})(K-1)T_p}\right]^T, \quad (5)$$

and $d_k(f_{d,m,n}(\theta_{m,n}, \boldsymbol{v}))$ denotes the k-th entry of $\boldsymbol{d}(f_{d,m,n}(\theta_{m,n}, \boldsymbol{v}))$.

Then, collecting the received signals from all Q_n antennas, we form $\boldsymbol{Y}_{m,n}(k) \in \mathbb{C}^{L\times Q_n}$ and

$$\boldsymbol{Y}_{m,n}(k) \triangleq \left[\boldsymbol{y}_{m,n,0}(k), \ldots, \boldsymbol{y}_{m,(n,q)}(k), \ldots, \boldsymbol{y}_{m,(n,Q_n-1)}(k)\right] = \alpha_{m,n} d_k(f_{d,m,n}(\theta_{m,n}, \boldsymbol{v}))\, \boldsymbol{S}_m \boldsymbol{a}_m(\theta_{m,n})\, \boldsymbol{b}_n^T(\theta_{m,n}), \quad (6)$$

$$\boldsymbol{y}_{m,n}(k) \triangleq \mathrm{vec}\{\boldsymbol{Y}_{m,n}(k)\} = \alpha_{m,n} d_k(f_{d,m,n}(\theta_{m,n}, \boldsymbol{v}))\, \boldsymbol{A}_{m,n}(\theta_{m,n})\, \boldsymbol{s}_m, \quad (7)$$

with

$$\boldsymbol{s}_m \triangleq \mathrm{vec}\{\boldsymbol{S}_m\}, \quad (8)$$

$$\boldsymbol{A}_{m,n}(\theta_{m,n}) \triangleq \left[\boldsymbol{b}_n(\theta_{m,n})\, \boldsymbol{a}_m^T(\theta_{m,n})\right] \otimes \boldsymbol{I}_L. \quad (9)$$

$$\begin{aligned}\boldsymbol{y}_{m,(n,q)}(k) &\triangleq \sum_{p=0}^{P_m-1} \alpha_{m,n} \boldsymbol{s}_{m,p} e^{-j2\pi f_c \tau_{(m,p),(n,q)}(\theta_{m,n})} e^{-j2\pi k T_p f_{d,m,n}(\theta_{m,n},\boldsymbol{v})} \\ &= \alpha_{m,n} b_{n,q}(\theta_{m,n})\, d_k(f_{d,m,n}(\theta_{m,n}, \boldsymbol{v})) \sum_{p=0}^{P_m-1} a_{m,p}(\theta_{m,n})\, \boldsymbol{s}_{m,p} \\ &= \alpha_{m,n} b_{n,q}(\theta_{m,n})\, d_k(f_{d,m,n}(\theta_{m,n}, \boldsymbol{v}))\, \boldsymbol{S}_m \boldsymbol{a}_m(\theta_{m,n}), \end{aligned} \quad (2)$$

Collecting all K pulses of $\boldsymbol{Y}_{m,n}(k)$, the received signal can be represented by an LKQ_n-dimensional vector

$$\begin{aligned}\boldsymbol{y}_{m,n} &\triangleq \left[\boldsymbol{y}_{m,n}^T(0),\ldots,\boldsymbol{y}_{m,n}^T(k),\ldots,\boldsymbol{y}_{m,n}^T(K-1)\right]^T \\ &= \alpha_{m,n}\underbrace{\boldsymbol{d}\left(f_{d,m,n}\left(\theta_{m,n},\boldsymbol{v}\right)\right)\otimes\left[\boldsymbol{A}_{m,n}\left(\theta_{m,n}\right)\boldsymbol{s}_m\right]}_{\boldsymbol{h}_{m,n}\left(\theta_{m,n},\boldsymbol{v}\right)}. \quad (10)\end{aligned}$$

After obtaining the above received signal from the target, the received signals from clutter scatterers can be similarly obtained. As shown in Fig. 1, the echo waveform from the target is interfered by that from the clutter in the same ellipse. Then, following the same derivation, the received signal from clutter can be expressed as

$$\boldsymbol{z}_{m,n} = \sum_{c=0}^{C_{m,n}-1}\beta_{m,n,c}\boldsymbol{h}_{m,n}\left(\zeta_{m,n,c}\right), \quad (11)$$

where $C_{m,n}$ is the number of clutter scatterers in the same ellipse, $\beta_{m,n,c}$ and $\zeta_{m,n,c}$ are respectively the scattering coefficient and angle of the c-th clutter. Since clutter is stationary, where we have $\boldsymbol{h}_{m,n}\left(\zeta_{m,n,c}\right) \triangleq \boldsymbol{h}_{m,n}\left(\zeta_{m,n,c},\boldsymbol{0}\right)$.

Finally the received signal by the n-th RX due to the transmitted signal from the m-th TX is given by

$$\begin{aligned}\boldsymbol{r}_{m,n} &= \boldsymbol{z}_{m,n}+\boldsymbol{y}_{m,n}+\boldsymbol{n}_{m,n} \\ &= \sum_{c=0}^{C_{m,n}-1}\beta_{m,n,c}\boldsymbol{h}_{m,n}\left(\zeta_{m,n,c}\right) \\ &\quad +\alpha_{m,n}\boldsymbol{h}_{m,n}\left(\theta_{m,n},\boldsymbol{v}\right)+\boldsymbol{n}_{m,n}, \quad (12)\end{aligned}$$

where $\boldsymbol{n}_{m,n}\sim\mathcal{CN}\left(\boldsymbol{0},\sigma_n^2\boldsymbol{I}_{LKQ_n}\right)$ is the additive white Gaussian noise (AWGN), σ_n^2 is the noise variance and LKQ_n is the length of the vector $\boldsymbol{r}_{m,n}$.

In this paper, we assume that the platform velocities ($\boldsymbol{v}_{T,m}$ and $\boldsymbol{v}_{R,n}$) and positions ($\boldsymbol{p}_{T,m}$ and $\boldsymbol{p}_{R,n}$) are known. Since we detect whether the moving target is present at the position intersected by ellipses as shown in Fig. 1, the target angle $\theta_{m,n}$ and position $\boldsymbol{p}$ are known. However, $\alpha_{m,n}$, $\boldsymbol{v}$, $\beta_{m,n,c}$, and $\zeta_{m,n,c}$ are all assumed unknown.

III. Moving Target Detection

In most existing works on MIMO radar, the radar is static and the target can be either static [39]–[41] or moving [4], [7], [14]. In [3], moving target detection with distributed moving MIMO radar platforms is considered, where there is only one antenna in each radar platform. Here, we propose a GLRT-based moving target detection method using multiple moving platforms with colocated MIMO antennas.

First, based on the signal model developed in the previous section, the detection problem can be expressed as

$$H_0:\boldsymbol{r}=\boldsymbol{z}+\boldsymbol{n} \quad (13)$$

$$H_1:\boldsymbol{r}=\boldsymbol{y}+\boldsymbol{z}+\boldsymbol{n}, \quad (14)$$

where H_0 and H_1 denote the hypotheses corresponding to the absence and presence of target, respectively. We define $\boldsymbol{r}\triangleq\mathrm{vec}\{\boldsymbol{R}\}$, $\boldsymbol{y}\triangleq\mathrm{vec}\{\boldsymbol{Y}\}$, $\boldsymbol{z}\triangleq\mathrm{vec}\{\boldsymbol{Z}\}$, $\boldsymbol{n}\triangleq\mathrm{vec}\{\boldsymbol{N}\}$, where

$$\boldsymbol{R}\triangleq\begin{pmatrix}\boldsymbol{r}_{0,0} & \boldsymbol{r}_{0,1} & \cdots & \boldsymbol{r}_{0,N-1}\\ \boldsymbol{r}_{1,0} & \boldsymbol{r}_{1,1} & \cdots & \boldsymbol{r}_{1,N-1}\\ \vdots & \vdots & \ddots & \vdots\\ \boldsymbol{r}_{M-1,0} & \boldsymbol{r}_{M-1,1} & \cdots & \boldsymbol{r}_{M-1,N-1}\end{pmatrix} \quad (15)$$

and $\boldsymbol{Y}$, $\boldsymbol{Z}$, and $\boldsymbol{N}$ are similarly defined.

In this paper, the clutter is location dependent, so the clutter interferences are non-homogeneous and changing with the moving radar platforms. Therefore, the characteristics of clutter distribution cannot be estimated from the adjacent areas without target, and the traditional methods for target detection based on the statistical information, such as covariance matrix or subspace detector [4], [7], [10], cannot be adopted. To overcome this problem, the GLRT detector is adopted, and the echo waveforms from target and clutter are estimated during the processes of target detection without using the statistical information of target and clutter. The GLRT detector has the following form

$$\mathcal{T}_{\mathrm{GLRT}}=\frac{\max_{\alpha,\boldsymbol{v},\beta,\zeta}p(\boldsymbol{r}\,|H_1,\alpha,\boldsymbol{v},\beta,\zeta)}{\max_{\beta,\zeta}p(\boldsymbol{r}\,|H_0,\beta,\zeta)}\underset{H_0}{\overset{H_1}{\gtrless}}\lambda_G, \quad (16)$$

where λ_G is the detection threshold, and

$$\alpha\triangleq\left\{\alpha_{m,n},0\le m\le M-1,0\le n\le N-1\right\}, \quad (17)$$

$$\beta\triangleq\left\{\beta_{m,n},0\le m\le M-1,0\le n\le N-1\right\}, \quad (18)$$

$$\zeta\triangleq\left\{\zeta_{m,n,c},0\le m\le M-1,0\le n\le N-1,\ 0\le c\le C_{m,n}-1\right\}. \quad (19)$$

Some special cases of the GLRT detector in (16) are as follows

1) *Static distributed MIMO radar:* Set the antenna numbers as $P_m=1\,(0\le m\le M-1)$ and $Q_n=1\,(0\le n\le N-1)$, and only consider the Doppler frequencies caused by moving target, which is considered in [7].
2) *Moving distributed MIMO radar:* Set the antenna numbers as $P_m=1\,(0\le m\le M-1)$ and $Q_n=1\,(0\le n\le N-1)$, and consider the Doppler frequencies caused by both moving radars and target, which is considered in [3].
3) *Colocated MIMO radar:* Set the radar platform numbers as $M=1$ and $N=1$, and consider the Doppler frequencies caused by both moving radars and target. The target estimation performance for this case is provided in [42].

So far no moving target detection method has been proposed for moving colocated MIMO radar and only the Cramér-Rao lower bound (CRLB) for the angular resolution is given in [42]. As a special case of (16), a GLRT detector is also proposed for moving distributed MIMO radar in [3]. The GLRT detector in (16) unifies both the colocated and distributed MIMO radars and can handle both static and moving radar platforms or target. Moreover, by introducing waveform optimization and employing more antennas in each moving radar platform, the detection performance can be further improved.

From (13) and (14), we have

$$\boldsymbol{r}\,|H_1,\boldsymbol{y},\boldsymbol{z}\ \sim\mathcal{CN}\left(\boldsymbol{y}+\boldsymbol{z},\sigma_n^2\boldsymbol{I}_{\sum_{n=1}^{N}MKLQ_n}\right), \tag{20}$$

$$\boldsymbol{r}\,|H_0,\boldsymbol{z}\ \sim\mathcal{CN}\left(\boldsymbol{z},\sigma_n^2\boldsymbol{I}_{\sum_{n=1}^{N}MKLQ_n}\right), \tag{21}$$

where $\sum_{n=1}^{N}MKLQ_n$ is the dimension of $\boldsymbol{r}$. Since $\boldsymbol{y}$ is a function of $(\alpha,\boldsymbol{v})$ and $\boldsymbol{z}$ is a function of (β,ζ), the GLR in (16) becomes

$$\mathcal{T}_{\text{GLR}}=\frac{\max_{\boldsymbol{y},\boldsymbol{z}}\ \exp\left(-\frac{1}{\sigma_n^2}g_1\left(\boldsymbol{r},\boldsymbol{z},\boldsymbol{y}\right)\right)}{\max_{\boldsymbol{z}}\ \exp\left(-\frac{1}{\sigma_n^2}g_0\left(\boldsymbol{r},\boldsymbol{z}\right)\right)}, \tag{22}$$

where we define $g_0\left(\boldsymbol{r},\boldsymbol{z}\right)\triangleq\|\boldsymbol{r}-\boldsymbol{z}\|_2^2$ and $g_1\left(\boldsymbol{r},\boldsymbol{z},\boldsymbol{y}\right)\triangleq\|\boldsymbol{r}-\boldsymbol{y}-\boldsymbol{z}\|_2^2$. Denote

$$\hat{\boldsymbol{z}}_0\triangleq\arg\min_{\boldsymbol{z}}\ g_0\left(\boldsymbol{r},\boldsymbol{z}\right), \tag{23}$$

$$\{\hat{\boldsymbol{z}}_1,\hat{\boldsymbol{y}}\}\triangleq\arg\min_{\boldsymbol{z},\boldsymbol{y}}\ g_1\left(\boldsymbol{r},\boldsymbol{z},\boldsymbol{y}\right). \tag{24}$$

Then, the GLRT detector in (16) becomes

$$g\left(\boldsymbol{r},\hat{\boldsymbol{z}}_0,\hat{\boldsymbol{z}}_1,\hat{\boldsymbol{y}}\right)\underset{H_0}{\overset{H_1}{\gtrless}}\lambda_G', \tag{25}$$

where

$$\begin{aligned}g\left(\boldsymbol{r},\hat{\boldsymbol{z}}_0,\hat{\boldsymbol{z}}_1,\hat{\boldsymbol{y}}\right)&\triangleq g_0\left(\boldsymbol{r},\hat{\boldsymbol{z}}_0\right)-g_1\left(\boldsymbol{r},\hat{\boldsymbol{z}}_1,\hat{\boldsymbol{y}}\right)\\&=2\,\text{Re}\left\{\boldsymbol{r}^H\left(\hat{\boldsymbol{y}}+\hat{\boldsymbol{z}}_1-\hat{\boldsymbol{z}}_0\right)-\hat{\boldsymbol{z}}_1^H\hat{\boldsymbol{y}}\right\}\\&\quad+\|\hat{\boldsymbol{z}}_0\|_2^2-\|\hat{\boldsymbol{z}}_1\|_2^2-\|\hat{\boldsymbol{y}}\|_2^2.\end{aligned} \tag{26}$$

The detection threshold λ_G is chosen according to a false alarm rate specified for the radar operation. The distribution of the generalized likelihood ratio can be obtained from simulations or experiments under the null hypothesis (i.e., no target is present). Then, the corresponding detection threshold λ_G can be obtained from the predetermined probability of false alarm.

IV. Echo Waveform Estimation

According to the data from the MIT Lincoln Laboratory Phase One radar [43] and the relative power of the eigenvalues in the clutter spectrum [44], the clutter spectrum of MIMO radar is dominated by the strong components which are sparse. Therefore, in this section, under the assumption that the clutter is distributed sparsely in the detection area, a CS-based model is proposed to describe the geographically sparse clutter and to estimate the echo waveforms in (23) and (24) via sparse reconstruction.

To detect the target, the parameters associated with the detection problem under both hypotheses, i.e., with the absence and presence of target, must be estimated first. This is a standard approach for detection, which essentially compares the two sets of estimates and selects the hypothesis that provides a better fitting to the data [45]. Then, the detection formula and the corresponding detection threshold in (16) can be obtained. Therefore, the parameters will be estimated under these two hypotheses in the following contents.

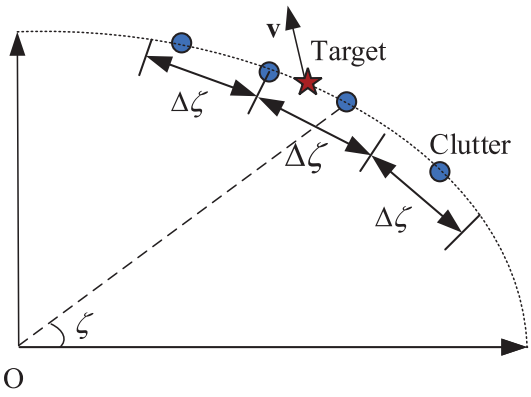

Fig. 3. The discretized angles.

A. Waveform Estimation With the Absence of Target

From (11) the echo waveform $\boldsymbol{z}_{m,n}$ is a function of clutter scattering coefficients and angles. As shown in Fig. 3, with an angle step $\Delta\zeta$, the clutter angle is discretized into a vector of size Z, $\boldsymbol{\zeta}=[\zeta_0,\zeta_1,\ldots,\zeta_{Z-1}]^T$. Then a dictionary containing all echo waveforms from the angles in $\boldsymbol{\zeta}$ can be obtained

$$\boldsymbol{H}_{m,n}\left(\boldsymbol{\zeta}\right)\triangleq\left[\boldsymbol{h}_{m,n}\left(\zeta_0\right),\boldsymbol{h}_{m,n}\left(\zeta_1\right),\ldots,\boldsymbol{h}_{m,n}\left(\zeta_{Z-1}\right)\right]. \tag{27}$$

Note that to form $\boldsymbol{H}_{m,n}\left(\boldsymbol{\zeta}\right)$, the following system parameters are assumed known:

- the transmitted waveforms $\boldsymbol{s}_m$,
- the platform velocities $\boldsymbol{v}_{T,m}$ and $\boldsymbol{v}_{R,n}$ and positions $\boldsymbol{p}_{T,m}$ and $\boldsymbol{p}_{R,n}$,
- the target angle $\theta_{m,n}$ and position $\boldsymbol{p}$,
- the detection angle $\boldsymbol{\zeta}$.

The clutter angles and scattering coefficients are not known and need to be estimated by CS reconstruction. However, the clutter may not be exactly on the discretized angle grid $\boldsymbol{\zeta}$. Therefore, the estimation problem of both scattering coefficients and angles becomes an off-grid CS problem [46], [47].

In particular for the c-th clutter, we can first approximate the off-grid echo waveform $\beta_{m,n,c}\boldsymbol{h}_{m,n}\left(\zeta_{m,n,c}\right)$ by the first-order Taylor series expansion [47], i.e.,

$$\beta_{m,n,c}\boldsymbol{h}_{m,n}\left(\zeta_{m,n,c}\right)\approx\beta_{m,n,c}\left[\boldsymbol{h}_{m,n}\left(\zeta_z\right)+\zeta'\nabla\boldsymbol{h}_{m,n}\left(\zeta_z\right)\right], \tag{28}$$

where $\nabla\boldsymbol{h}_{m,n}\left(\zeta_z\right)\triangleq\left.\frac{\partial\boldsymbol{h}_{m,n}(\zeta)}{\partial\zeta}\right|_{\zeta=\zeta_z}$, and $-\frac{\Delta\zeta}{2}\le\zeta'<\frac{\Delta\zeta}{2}$ is the off-grid angle. Then, the clutter angle $\zeta_{m,n,c}$ can be approximated by

$$\zeta_{m,n,c}\approx\zeta_z+\zeta'. \tag{29}$$

Therefore, the echo waveforms from clutter in (11) can be rewritten as the off-grid CS model

$$\boldsymbol{z}_{m,n}=\boldsymbol{H}_{m,n}\left(\boldsymbol{\zeta}\right)\boldsymbol{x}_{m,n}+\nabla\boldsymbol{H}_{m,n}\left(\boldsymbol{\zeta}\right)\left(\boldsymbol{p}_{m,n}\odot\boldsymbol{x}_{m,n}\right), \tag{30}$$

where $\odot$ denotes the Hadamard product (entry-wise product), $\boldsymbol{x}_{m,n}$ is a sparse vector and the nonzero entries indicate the scattering coefficients, $\boldsymbol{p}_{m,n}$ is the corresponding sparse vector indicating the off-grid angle. For example, in (28), the scattering coefficient $\beta_{m,n,c}$ of the c-th clutter corresponds to the z-th entry $x_{m,n,z}=\beta_{m,n,c}$ in $\boldsymbol{x}_{m,n}$, and the off-grid angle ζ' corresponds to the z-th entry $p_{m,n,z}=\zeta'$ in $\boldsymbol{p}_{m,n}$.

Then the received signal in (13) can be rewritten as

$$\boldsymbol{r}_{m,n} = \underbrace{\left(\boldsymbol{H}_{m,n}\left(\boldsymbol{\zeta}\right), \triangledown \boldsymbol{H}_{m,n}\left(\boldsymbol{\zeta}\right)\right)}_{\boldsymbol{\Phi}_{m,n}} \begin{pmatrix} \boldsymbol{x}_{m,n} \\ \boldsymbol{t}_{m,n} \end{pmatrix} + \boldsymbol{n}_{m,n}, \quad (31)$$

where $\boldsymbol{t}_{m,n} \triangleq \boldsymbol{p}_{m,n} \odot \boldsymbol{x}_{m,n}$. The echo waveform estimation then becomes the reconstruction of the sparse vectors $\boldsymbol{x}_{m,n}$ and $\boldsymbol{p}_{m,n}$. The JOMP algorithm in [33], can be adapted to reconstruct the sparse vector $\left(\boldsymbol{x}_{m,n}^T, \boldsymbol{t}_{m,n}^T\right)^T$ where $\boldsymbol{x}_{m,n}$ and $\boldsymbol{p}_{m,n}$ have the same support.

However, in the JOMP algorithm, the matrices $\boldsymbol{H}_{m,n}\left(\boldsymbol{\zeta}\right)$ and $\triangledown \boldsymbol{H}_{m,n}\left(\boldsymbol{\zeta}\right)$ are treated with equal importance. On the other hand it is more appropriate to reconstruct the sparse vector according to the dictionary matrix $\boldsymbol{H}_{m,n}\left(\boldsymbol{\zeta}\right)$ and estimate the off-grid angles via the derivative matrix $\triangledown \boldsymbol{H}_{m,n}\left(\boldsymbol{\zeta}\right)$. Therefore, inspired by alternating minimization and CS dictionary learning [48], [49], a two-step OMP algorithm is proposed here to reconstruct $\boldsymbol{x}_{m,n}$ and $\boldsymbol{p}_{m,n}$. The reason why we develop an algorithm based on OMP is the proposed algorithm can achieve good performance while inherits the good efficiency of the OMP algorithm, compared with NESTA [50], OGSBI [47] and other algorithms. Therefore, the two-step OMP can obtain a good trade-off between the estimation performance and the computational complexity.

Define $\boldsymbol{X}_{m,n} \triangleq \mathrm{diag}\left\{\boldsymbol{x}_{m,n}\right\}$. Then (31) can be written as

$$\boldsymbol{r}_{m,n} = \boldsymbol{H}_{m,n}\left(\boldsymbol{\zeta}\right)\boldsymbol{x}_{m,n} + \left[\triangledown \boldsymbol{H}_{m,n}\left(\boldsymbol{\zeta}\right)\boldsymbol{X}_{m,n}\right]\boldsymbol{p}_{m,n} + \boldsymbol{n}_{m,n}. \quad (32)$$

The proposed algorithm iterates between the following two steps:

1) Use the dictionary matrix $\boldsymbol{H}_{m,n}\left(\boldsymbol{\zeta}\right)$ to reconstruct the sparse vector $\boldsymbol{x}_{m,n}$, by treating the last two terms $\left[\triangledown \boldsymbol{H}_{m,n}\left(\boldsymbol{\zeta}\right)\boldsymbol{X}_{m,n}\right]\boldsymbol{p}_{m,n} + \boldsymbol{n}_{m,n}$ in (32) as noise. The reconstructed sparse vector is denoted as $\hat{\boldsymbol{x}}_{m,n}$ with support Λ.
2) Denote $\hat{\boldsymbol{X}}_\Lambda \triangleq \mathrm{diag}\left\{\hat{\boldsymbol{x}}_{m,n,\Lambda}\right\}$, the matrix $\triangledown \boldsymbol{H}_{m,n,\Lambda}\left(\boldsymbol{\zeta}\right)\hat{\boldsymbol{X}}_\Lambda$ serves as the new dictionary and is used to estimate the off-grid angle $\hat{\boldsymbol{p}}_{m,n,\Lambda}$ from $\left(\boldsymbol{r}_{m,n} - \boldsymbol{H}_{m,n,\Lambda}\left(\boldsymbol{\zeta}\right)\hat{\boldsymbol{x}}_{m,n,\Lambda}\right)$. Therefore, the second step is not a sparse estimation problem, and $\hat{\boldsymbol{x}}_{m,n}$ and $\hat{\boldsymbol{p}}_{m,n}$ have the same support Λ. Here $\boldsymbol{x}_\Lambda$ denotes the subvector of $\boldsymbol{x}$ corresponding to the elements with indices in Λ, and $\boldsymbol{H}_{m,n,\Lambda}$ denotes a sub-dictionary matrix of $\boldsymbol{H}_{m,n}$ with column indices in Λ.

The detailed procedure is given in Algorithm 1. The computational complexity of the proposed method in one iteration is $\mathcal{O}(ZLKQ_nC_{m,n}) + \mathcal{O}(C_{m,n})$. Moreover, Algorithm 1 is different from applying the OMP method twice. The OMP-based method cannot handle the off-grid reconstruction problem, where the clutter cannot be exactly at the discretized grids, and the traditional OMP method can only solve the sparse reconstruction problem with the assumption that the non-zero elements are exactly on the discretized grids. However, Algorithm 1 can estimate the sparse clutter with the off-grid assumption, and further improve the clutter estimation performance.

The estimated echo waveform from clutter is then

$$\hat{\boldsymbol{z}}_{m,n} = \boldsymbol{H}_{m,n}\left(\hat{\boldsymbol{\zeta}}\right)\hat{\boldsymbol{x}}_{m,n} + \triangledown \boldsymbol{H}_{m,n}\left(\boldsymbol{\zeta}\right)\mathrm{diag}\left\{\hat{\boldsymbol{x}}_{m,n}\right\}\hat{\boldsymbol{p}}_{m,n}. \quad (33)$$

Finally we form $\hat{\boldsymbol{Z}} = \left[\hat{\boldsymbol{z}}_{m,n}\right]$ $(0 \le m \le M-1, 0 \le n \le N-1)$ and the estimated clutter waveform in (26) is given by $\hat{\boldsymbol{z}}_0 = \mathrm{vec}\{\hat{\boldsymbol{Z}}\}$.

Algorithm 1: Proposed Algorithm for Solving (23).

Input: dictionary matrix $\boldsymbol{H}_{m,n}\left(\boldsymbol{\zeta}\right)$, derivative matrix $\triangledown \boldsymbol{H}_{m,n}\left(\boldsymbol{\zeta}\right)$, received signal $\boldsymbol{r}_{m,n}$, stopping threshold ϵ, maximum iteration number K_I, number of discretized angles Z.
Initialization: $\hat{\boldsymbol{p}}_{m,n} = \boldsymbol{0}$, $\boldsymbol{r}_1 = \boldsymbol{r}_{m,n}$, and normalize each column of $\boldsymbol{H}_{m,n}\left(\boldsymbol{\zeta}\right)$.
for $k_I = 1$ to K_I **do**
  $\Lambda \leftarrow \emptyset$, and $\boldsymbol{b} \leftarrow \boldsymbol{r}_1$.
  for $k_I' = 1$ to Z **do**
    $\Lambda \leftarrow \Lambda \cup \lambda$, where $\lambda = \arg\max_i \left|\left[\boldsymbol{H}_{m,n}^H(\boldsymbol{\zeta})\boldsymbol{b}\right]_i\right|^2$.
    $\hat{\boldsymbol{x}}_{m,n,\Lambda} = \arg\min_{\boldsymbol{x}_{m,n,\Lambda}} \left\|\boldsymbol{r}_1 - \boldsymbol{H}_{m,n,\Lambda}\left(\boldsymbol{\zeta}\right)\boldsymbol{x}_{m,n,\Lambda}\right\|_2^2$.
    $\boldsymbol{b} = \boldsymbol{r}_1 - \boldsymbol{H}_{m,n,\Lambda}\left(\boldsymbol{\zeta}\right)\hat{\boldsymbol{x}}_{m,n,\Lambda}$.
    if $\|\boldsymbol{b}\|_2^2 \le \epsilon$ **then**
      Break.
    end if
  end for
  $\boldsymbol{r}_2 = \boldsymbol{r}_{m,n} - \boldsymbol{H}_{m,n,\Lambda}\left(\boldsymbol{\zeta}\right)\hat{\boldsymbol{x}}_{m,n,\Lambda}$, $\boldsymbol{D}_\Lambda = \triangledown \boldsymbol{H}_{m,n,\Lambda}\left(\boldsymbol{\zeta}\right)\mathrm{diag}\left\{\hat{\boldsymbol{x}}_{m,n,\Lambda}\right\}$.
  $\hat{\boldsymbol{p}}_{m,n,\Lambda} = \arg\min_{\boldsymbol{p}_{m,n,\Lambda}} \left\|\boldsymbol{r}_2 - \boldsymbol{D}_\Lambda\boldsymbol{p}_{m,n,\Lambda}\right\|_2^2$ s.t. $-\frac{\Delta\zeta}{2} \le p_{m,n,i} < \frac{\Delta\zeta}{2}, \forall i \in \Lambda$.
  $\boldsymbol{r}_1 = \boldsymbol{r}_{m,n} - \boldsymbol{D}_\Lambda\hat{\boldsymbol{p}}_{m,n,\Lambda}$.
end for
Output: reconstructed sparse vector $\hat{\boldsymbol{x}}_{m,n}$ and $\hat{\boldsymbol{p}}_{m,n}$.

B. Waveform Estimation With the Presence of Target

Since the received signal now is the superposition of waveforms from both clutter and target, an iterative algorithm can be used to estimate $\hat{\boldsymbol{z}}_1$ and $\hat{\boldsymbol{y}}$ in (24) as given in Algorithm 2.

At Step 4 of Algorithm 2, due to the target movement, the target velocity $\boldsymbol{v}$ needs to be estimated first. We can discretize the target velocity and obtain the estimated velocity $\hat{\boldsymbol{v}}$ by minimizing the orthogonal projections. Then, the target scattering coefficient can be estimated as $\hat{\alpha}_{m,n}$. The target component of the received signal can be obtained as $\hat{\boldsymbol{y}}_{m,n} = \hat{\alpha}_{m,n}\boldsymbol{h}_{m,n}(\theta_{m,n}, \hat{\boldsymbol{v}})$. Then, using our Algorithm 1, $\hat{\boldsymbol{z}}_1$ can be obtained from $\boldsymbol{r} - \hat{\boldsymbol{y}}$. Next, we can re-estimate the target waveform $\hat{\boldsymbol{y}}$ from $\boldsymbol{r} - \hat{\boldsymbol{z}}_1$. Iterate these steps until reaching the stopping criterion.

Finally, given the estimates $\hat{\boldsymbol{y}}$, $\hat{\boldsymbol{z}}_1$ and $\hat{\boldsymbol{z}}_0$, the GLRT detector in (25) can be computed. Moreover, in such a case with additional scatterers simultaneously in the same range resolution cell and antenna main beam, the target detection method can be also used.

V. Waveform Optimization

In the GLRT detector, the scattering coefficients and angles of both target and clutter are estimated. Based on these estimates, we can further improve the target detection performance by online optimizing the transmitted waveforms

$\{\boldsymbol{s}_{m,p}, m = 0, \ldots, M-1, p = 0, \ldots, P_m - 1\}$. In particular, for each TX m, we can maximize the SCNR under the transmit power constraint. Since all RXs can receive the waveforms transmitted by the m-th TX, the SCNR for the m-th TX can be measured by using the received signals at all RXs.

A. Problem Formulation

As stated in Section IV, the clutter sparse vector $\hat{\boldsymbol{x}}_{m,n}$ and off-grid vector $\hat{\boldsymbol{p}}_{m,n}$ can be reconstructed using Algorithm 1. Then, the clutter scattering coefficients $\hat{\boldsymbol{\beta}}_{m,n}$ and angles $\hat{\boldsymbol{\zeta}}_{m,n}$ can be obtained from the nonzero entries of $\hat{\boldsymbol{x}}_{m,n}$ and $\hat{\boldsymbol{p}}_{m,n}$ respectively. Additionally, the target scattering coefficient $\hat{\alpha}_{m,n}$ and velocity $\hat{\boldsymbol{v}}$ are estimated using Algorithm 2. Using (9)-(10), the power of the target echo waveform is given in (34) shown at the bottom of the page, where we have used the following identities:

$$(\boldsymbol{A} \otimes \boldsymbol{B})^H = \boldsymbol{A}^H \otimes \boldsymbol{B}^H, \tag{36}$$

$$(\boldsymbol{A} \otimes \boldsymbol{B})(\boldsymbol{C} \otimes \boldsymbol{D}) = \boldsymbol{AC} \otimes \boldsymbol{BD}, \tag{37}$$

$$\mathrm{Tr}\{\boldsymbol{AXB}\} = (\boldsymbol{B}^H \otimes \boldsymbol{A})\,\mathrm{vec}\{\boldsymbol{X}\}, \tag{38}$$

$$\mathrm{Tr}\left\{\boldsymbol{A}^H\boldsymbol{Y}\right\} = \mathrm{vec}\{\boldsymbol{A}\}^H\,\mathrm{vec}\{\boldsymbol{Y}\}. \tag{39}$$

Similarly, the total power of the clutter echo waveforms can be obtained from (11), as (35) shown at the bottom of the page.

$$\begin{aligned}
P_{T,m,n} &= \left\|\boldsymbol{y}_{m,n}\right\|_2^2 \\
&= |\alpha_{m,n}|^2 \left\{\boldsymbol{d}\left(f_{d,m,n}\left(\theta_{m,n}, \boldsymbol{v}\right)\right) \otimes \left[\boldsymbol{A}_{m,n}\left(\theta_{m,n}\right)\boldsymbol{s}_m\right]\right\}^H \left\{\boldsymbol{d}\left(f_{d,m,n}\left(\theta_{m,n}, \boldsymbol{v}\right)\right) \otimes \left[\boldsymbol{A}_{m,n}\left(\theta_{m,n}\right)\boldsymbol{s}_m\right]\right\} \\
&\overset{(37)}{=} |\alpha_{m,n}|^2 \left\{\boldsymbol{d}^H\left(f_{d,m,n}\left(\theta_{m,n}, \boldsymbol{v}\right)\right)\boldsymbol{d}\left(f_{d,m,n}\left(\theta_{m,n}, \boldsymbol{v}\right)\right)\right\} \otimes \left\{\left[\boldsymbol{A}_{m,n}\left(\theta_{m,n}\right)\boldsymbol{s}_m\right]^H\left[\boldsymbol{A}_{m,n}\left(\theta_{m,n}\right)\boldsymbol{s}_m\right]\right\} \\
&= |\alpha_{m,n}|^2 \left\|\boldsymbol{d}^H\left(f_{d,m,n}\left(\theta_{m,n}, \boldsymbol{v}\right)\right)\right\|_2^2 \boldsymbol{s}_m^H\left\{\left[\boldsymbol{b}_n\left(\theta_{m,n}\right)\boldsymbol{a}_m^T\left(\theta_{m,n}\right)\right] \otimes \boldsymbol{I}_L\right\}^H\left\{\left[\boldsymbol{b}_n\left(\theta_{m,n}\right)\boldsymbol{a}_m^T\left(\theta_{m,n}\right)\right] \otimes \boldsymbol{I}_L\right\}\boldsymbol{s}_m \\
&\overset{(37)}{=} \underbrace{|\alpha_{m,n}|^2 \left\|\boldsymbol{d}\left(f_{d,m,n}(\theta_{m,n}, \boldsymbol{v})\right)\right\|_2^2 \left\|\boldsymbol{b}_n(\theta_{m,n})\right\|_2^2}_{u_{m,n}} \boldsymbol{s}_m^H\left[\left(\boldsymbol{a}_m(\theta_{m,n})\boldsymbol{a}_m^H(\theta_{m,n})\right)^T \otimes \boldsymbol{I}_L\right]\boldsymbol{s}_m \\
&= \boldsymbol{s}_m^H\Big[\underbrace{u_{m,n}\left(\boldsymbol{a}_m(\theta_{m,n})\boldsymbol{a}_m^H(\theta_{m,n})\right)^T}_{\boldsymbol{T}_{m,n}} \otimes \boldsymbol{I}_L\Big]\boldsymbol{s}_m \\
&\overset{(38)}{=} \boldsymbol{s}_m^H\,\mathrm{vec}\left\{\boldsymbol{S}_m\boldsymbol{T}_{m,n}^T\right\} \\
&\overset{(39)}{=} \mathrm{Tr}\left\{\boldsymbol{S}_m^H\boldsymbol{S}_m\boldsymbol{T}_{m,n}^T\right\}.
\end{aligned} \tag{34}$$

$$\begin{aligned}
P_{C,m,n} &= \left\|\boldsymbol{z}_{m,n}\right\|_2^2 \\
&= \left\{\sum_{c=0}^{C_{m,n}-1} \beta_{m,n,c}\boldsymbol{d}\left(f_{d,m,n}\left(\zeta_{m,n,c}\right)\right) \otimes \left[\left(\left(\boldsymbol{b}_n\left(\zeta_{m,n,c}\right)\boldsymbol{a}_m^T\left(\zeta_{m,n,c}\right)\right) \otimes \boldsymbol{I}_L\right)\boldsymbol{s}_m\right]\right\}^H \\
&\quad \left\{\sum_{c=0}^{C_{m,n}-1} \beta_{m,n,c}\boldsymbol{d}\left(f_{d,m,n}\left(\zeta_{m,n,c}\right)\right) \otimes \left[\left(\left(\boldsymbol{b}_n\left(\zeta_{m,n,c}\right)\boldsymbol{a}_m^T\left(\zeta_{m,n,c}\right)\right) \otimes \boldsymbol{I}_L\right)\boldsymbol{s}_m\right]\right\} \\
&= \sum_{c1=0}^{C_{m,n}-1}\sum_{c2=0}^{C_{m,n}-1} \underbrace{\beta_{m,n,c2}\beta_{m,n,c1}^H\boldsymbol{d}^H\left(f_{d,m,n}\left(\zeta_{m,n,c1}\right)\right)\boldsymbol{d}\left(f_{d,m,n}\left(\zeta_{m,n,c2}\right)\right)\left[\boldsymbol{b}_n^H\left(\zeta_{m,n,c1}\right)\boldsymbol{b}_n\left(\zeta_{m,n,c2}\right)\right]}_{v_{c_1,c_2}} \\
&\quad \boldsymbol{s}_m^H\left(\left[\boldsymbol{a}_m\left(\zeta_{m,n,c2}\right)\boldsymbol{a}_m^H\left(\zeta_{m,n,c1}\right)\right]^T \otimes \boldsymbol{I}_L\right)\boldsymbol{s}_m \\
&= \boldsymbol{s}_m^H\Bigg(\underbrace{\sum_{c1=0}^{C_{m,n}-1}\sum_{c2=0}^{C_{m,n}-1} v_{c_1,c_2}\left[\boldsymbol{a}_m\left(\zeta_{m,n,c2}\right)\boldsymbol{a}_m^H\left(\zeta_{m,n,c1}\right)\right]^T}_{\boldsymbol{C}_{m,n}} \otimes \boldsymbol{I}_L\Bigg)\boldsymbol{s}_m \\
&= \boldsymbol{s}_m^H\,\mathrm{vec}\left\{\boldsymbol{S}_m\boldsymbol{C}_{m,n}^T\right\} \\
&= \mathrm{Tr}\left\{\boldsymbol{S}_m^H\boldsymbol{S}_m\boldsymbol{C}_{m,n}^T\right\}.
\end{aligned} \tag{35}$$

Algorithm 2: Proposed Iterative Algorithm for Solving (24).

Input: dictionary matrix $\boldsymbol{H}_{m,n}(\boldsymbol{\zeta})$, derivative matrix $\nabla\boldsymbol{H}_{m,n}(\boldsymbol{\zeta})$, received signal $\boldsymbol{r}_{m,n}$, stopping threshold ϵ, maximum iteration number K_I.
Initialization: $\hat{\boldsymbol{z}}_{1,m,n}=\boldsymbol{0}_{LKQ_n}$, and normalize each column of $\boldsymbol{H}_{m,n}(\boldsymbol{\zeta})$.
for $k_I=1$ to K_I **do**
  $\hat{\boldsymbol{v}}=\arg\min_{\boldsymbol{v}}\sum_{m=0}^{M-1}\sum_{n=0}^{N-1}\left\|\boldsymbol{P}^{\perp}(\boldsymbol{h}_{m,n}(\theta_{m,n},\boldsymbol{v}))(\boldsymbol{r}_{m,n}-\hat{\boldsymbol{z}}_{1,m,n})\right\|_2^2$ where $\boldsymbol{P}^{\perp}(\boldsymbol{h}_{m,n}(\theta_{m,n},\boldsymbol{v}))\triangleq\boldsymbol{I}_{LKQ_n}-\frac{\boldsymbol{h}_{m,n}(\theta_{m,n},\boldsymbol{v})\boldsymbol{h}_{m,n}^H(\theta_{m,n},\boldsymbol{v})}{\boldsymbol{h}_{m,n}^H(\theta_{m,n},\boldsymbol{v})\boldsymbol{h}_{m,n}(\theta_{m,n},\boldsymbol{v})}$.
  for $m=0,\ldots,M-1$ and $n=0,\ldots,N-1$ **do**
    $\hat{\alpha}_{m,n}=\frac{\boldsymbol{h}_{m,n}^H(\theta_{m,n},\hat{\boldsymbol{v}})(\boldsymbol{r}_{m,n}-\hat{\boldsymbol{z}}_{1,m,n})}{\boldsymbol{h}_{m,n}^H(\theta_{m,n},\hat{\boldsymbol{v}})\boldsymbol{h}_{m,n}(\theta_{m,n},\hat{\boldsymbol{v}})}$.
    $\hat{\boldsymbol{y}}_{m,n}=\hat{\alpha}_{m,n}\boldsymbol{h}_{m,n}(\theta_{m,n},\hat{\boldsymbol{v}})$.
    Using Algorithm 1, reconstruct $\hat{\boldsymbol{x}}_{m,n}$ and $\hat{\boldsymbol{p}}_{m,n}$ from $(\boldsymbol{r}_{m,n}-\hat{\boldsymbol{y}}_{m,n})$.
    $\hat{\boldsymbol{z}}_{1,m,n}=\nabla\boldsymbol{H}_{m,n}(\boldsymbol{\zeta})\,\mathrm{diag}\{\hat{\boldsymbol{x}}_{m,n}\}\hat{\boldsymbol{p}}_{m,n}+\boldsymbol{H}_{m,n}(\boldsymbol{\zeta})\hat{\boldsymbol{x}}_{m,n}$.
  end for
  $\hat{\boldsymbol{y}}=\mathrm{vec}\{[\hat{\boldsymbol{y}}_{m,n}]\}$.
  $\hat{\boldsymbol{z}}_1=\mathrm{vec}\{[\hat{\boldsymbol{z}}_{1,m,n}]\}$.
  if $\|\boldsymbol{r}-\hat{\boldsymbol{y}}-\hat{\boldsymbol{z}}_1\|_2^2\le\epsilon$ **then**
    Break.
  end if
end for
Output: estimated clutter echo waveform $\hat{\boldsymbol{z}}_1$, target scattering coefficient $\hat{\alpha}_{m,n}$ and velocity $\hat{\boldsymbol{v}}$, target echo waveform $\hat{\boldsymbol{y}}$.

For the m-th TX, collecting the received signals by all RXs which are sent to the fusion center, the total power of clutter echo is

$$P_{C,m}=\sum_{n=0}^{N-1}P_{C,m,n}=\mathrm{Tr}\left\{\boldsymbol{S}_m^H\boldsymbol{S}_m\Big(\underbrace{\sum_{n=0}^{N-1}\boldsymbol{C}_{m,n}}_{\boldsymbol{C}_m}\Big)^T\right\}=\mathrm{Tr}\left\{\boldsymbol{S}_m^H\boldsymbol{S}_m\boldsymbol{C}_m^T\right\}. \tag{40}$$

The power of the target echo is

$$P_{T,m}=\sum_{n=0}^{N-1}P_{T,m,n}=\mathrm{Tr}\left\{\boldsymbol{S}_m^H\boldsymbol{S}_m\left(\underbrace{\sum_{n=0}^{N-1}\boldsymbol{T}_{m,n}}_{\boldsymbol{T}_m}\right)^T\right\}=\mathrm{Tr}\left\{\boldsymbol{S}_m^H\boldsymbol{S}_m\boldsymbol{T}_m^T\right\}. \tag{41}$$

Therefore, the SCNR for the m-th TX can be expressed as [3], [25]

$$f_m(\boldsymbol{S}_m)=\frac{P_{T,m}}{P_{C,m}+P_{N,m}}=\frac{\mathrm{Tr}\left\{\boldsymbol{S}_m^H\boldsymbol{S}_m\boldsymbol{T}_m^T\right\}}{\mathrm{Tr}\left\{\boldsymbol{S}_m^H\boldsymbol{S}_m\boldsymbol{C}_m^T\right\}+P_{N,m}}, \tag{42}$$

where the noise power $P_{N,m}=\sigma_n^2LK\sum_{n=0}^{N-1}Q_n$. Then, the waveform optimization problem for the m-th TX can be written as

$$\max_{\boldsymbol{S}_m} f_m(\boldsymbol{S}_m)\quad \text{s.t. } \mathrm{Tr}\left\{\boldsymbol{S}_m^H\boldsymbol{S}_m\right\}\le E_s, \tag{43}$$

where E_s is the power constraint of the m-th TX.

B. Solving the Waveform Optimization Problem

To solve the waveform optimization problem in (43), we rewrite it as

$$\max_{\boldsymbol{W}_m} f_m(\boldsymbol{W}_m)=\frac{\mathrm{Tr}\{\boldsymbol{T}_m\boldsymbol{W}_m\}}{\mathrm{Tr}\{\boldsymbol{C}_m\boldsymbol{W}_m\}+P_{N,m}}\quad \text{s.t. } \mathrm{Tr}\{\boldsymbol{W}_m\}\le E_s,\ \boldsymbol{W}_m\triangleq(\boldsymbol{S}_m^H\boldsymbol{S}_m)^T. \tag{44}$$

Note that the optimal solution satisfies $\mathrm{Tr}\{\boldsymbol{W}_m\}=E_s$. To see this, suppose otherwise $\mathrm{Tr}\{\boldsymbol{W}_m\}<E_s$ and define $\gamma=\frac{E_s}{\mathrm{Tr}\{\boldsymbol{W}_m\}}>1$, $\boldsymbol{W}'_m=\gamma\boldsymbol{W}_m$. Then $\mathrm{Tr}\{\boldsymbol{W}'_m\}=E_s$, $f_m(\boldsymbol{W}'_m)>f_m(\boldsymbol{W}_m)$.

Thus, the objective function in (44) can be simplified as

$$f_m(\boldsymbol{W}_m)=\frac{\mathrm{Tr}\{\boldsymbol{T}_m\boldsymbol{W}_m\}}{\mathrm{Tr}\{\boldsymbol{C}_m\boldsymbol{W}_m\}+\frac{P_{N,m}}{E_s}\mathrm{Tr}\{\boldsymbol{W}_m\}}=\frac{\mathrm{Tr}\{\boldsymbol{T}_m\boldsymbol{W}_m\}}{\mathrm{Tr}\left\{\left(\boldsymbol{C}_m+\frac{P_{N,m}}{E_s}\boldsymbol{I}_{P_m}\right)\boldsymbol{W}_m\right\}}. \tag{45}$$

Defining $\boldsymbol{D}_m\triangleq\boldsymbol{C}_m+\frac{P_{N,m}}{E_s}\boldsymbol{I}_{P_m}$, the waveform optimization problem can be expressed as

$$\max_{\boldsymbol{W}_m} f_m(\boldsymbol{W}_m)=\frac{\mathrm{Tr}\{\boldsymbol{T}_m\boldsymbol{W}_m\}}{\mathrm{Tr}\{\boldsymbol{D}_m\boldsymbol{W}_m\}}\quad \text{s.t. } \mathrm{Tr}\{\boldsymbol{W}_m\}=E_s,\ \mathrm{Rank}\{\boldsymbol{W}_m\}\le L,\ \boldsymbol{W}_m\succeq\boldsymbol{0}, \tag{46}$$

where the rank and semidefinite constraints ensure that $\boldsymbol{W}_m$ can be decomposed as $\boldsymbol{W}_m^T=\boldsymbol{S}_m^H\boldsymbol{S}_m$. In (46), the objective function is a quasiconvex linear-fractional function [51], and all the constraints except for the rank constraint are convex. Since $\boldsymbol{W}_m=(\boldsymbol{S}_m^H\boldsymbol{S}_m)^T\in\mathbb{C}^{P_m\times P_m}$ and $\mathrm{Rank}\{\boldsymbol{W}_m\}\le P_m$, we consider the following two cases.

1) If $P_m\le L$, we have

$$\mathrm{Rank}\{\boldsymbol{W}_m\}\le P_m\le L. \tag{47}$$

Then, the rank constraint can be removed, and we have the following optimization problem

$$\max_{\boldsymbol{W}_m} f_m(\boldsymbol{W}_m)=\frac{\mathrm{Tr}\{\boldsymbol{T}_m\boldsymbol{W}_m\}}{\mathrm{Tr}\{\boldsymbol{D}_m\boldsymbol{W}_m\}}\quad \text{s.t. } \mathrm{Tr}\{\boldsymbol{W}_m\}=E_s,\ \boldsymbol{W}_m\succeq\boldsymbol{0}, \tag{48}$$

By defining $\boldsymbol{X}_m = \frac{\boldsymbol{W}_m}{\mathrm{Tr}\{\boldsymbol{D}_m \boldsymbol{W}_m\}}$ and $d_m = \frac{1}{\mathrm{Tr}\{\boldsymbol{D}_m \boldsymbol{W}_m\}}$, an equivalent linear objective function can be obtained by the Charnes-Cooper transformation [52] as

$$\begin{aligned} \max_{\boldsymbol{X}_m, d_m} \quad & \mathrm{Tr}\{\boldsymbol{T}_m \boldsymbol{X}_m\} \\ \text{s.t.} \quad & \mathrm{Tr}\{\boldsymbol{D}_m \boldsymbol{X}_m\} = 1 \\ & \mathrm{Tr}\{\boldsymbol{X}_m\} = d_m E_s \\ & d_m \geq 0 \\ & \boldsymbol{X}_m \succeq \boldsymbol{0}. \end{aligned} \tag{49}$$

Since the convex optimization problem (49) is an SDP problem [53], it can be solved efficiently by the CVX toolbox [54] or the interior point method [51], [56]. Then, the optimal solution to (48) is

$$\boldsymbol{W}_m = \frac{1}{d_m} \boldsymbol{X}_m. \tag{50}$$

With the eigen-decomposition

$$\begin{aligned} \boldsymbol{W}_m &= \sum_{i=0}^{\Gamma_m - 1} \lambda_{m,i} \boldsymbol{v}_{m,i} \boldsymbol{v}_{m,i}^H + \sum_{i=\Gamma_m - 1}^{L-1} \boldsymbol{0}_{P_m \times P_m} \\ &= (\boldsymbol{S}^H \boldsymbol{S})^T \end{aligned} \tag{51}$$

where $\Gamma_m = \mathrm{Rank}\{\boldsymbol{W}_m\}$, $\lambda_{m,i}$ and $\boldsymbol{v}_{m,i}$ are the i-th largest eigenvalue and eigenvector, respectively. The optimal waveform matrix is

$$\begin{aligned} \boldsymbol{S}_m = \big(&\sqrt{\lambda_{m,0}} \boldsymbol{v}_{m,0}, \sqrt{\lambda_{m,1}} \boldsymbol{v}_{m,1}, \ldots, \\ &\sqrt{\lambda_{m,\Gamma_m - 1}} \boldsymbol{v}_{m,\Gamma_m - 1}, \boldsymbol{0}_{P_m \times (L - \Gamma_m)}\big)^T. \end{aligned} \tag{52}$$

2) If $P_m > L$, similarly, we first remove the rank constraint $\mathrm{Rank}\{\boldsymbol{W}_m\} \leq L$, and solve the relaxed problem in (48) to obtain (50) and (51).
   a) If $\Gamma_m \leq L$, the relaxed problem provides the optimal solution and the optimal waveform matrix is

$$\begin{aligned} \boldsymbol{S}_m = \big(&\sqrt{\lambda_{m,0}} \boldsymbol{v}_{m,0}, \sqrt{\lambda_{m,1}} \boldsymbol{v}_{m,1}, \ldots, \\ &\sqrt{\lambda_{m,\Gamma_m - 1}} \boldsymbol{v}_{m,\Gamma_m - 1}, \boldsymbol{0}_{P_m \times (L - \Gamma_m)}\big)^T. \end{aligned} \tag{53}$$

   b) If $\Gamma_m > L$, a suboptimal solution is given by the L eigenvectors corresponding to the L largest eigenvalues

$$\boldsymbol{S}_m = p_m \left(\sqrt{\lambda_{m,0}} \boldsymbol{v}_{m,0}, \ldots, \sqrt{\lambda_{m,L-1}} \boldsymbol{v}_{m,L-1}\right)^T, \tag{54}$$

   where the parameter p_m is used to ensure that $\mathrm{Tr}\{\boldsymbol{S}_m^H \boldsymbol{S}_m\} = E_s$.

VI. Simulation Results

In this section, we provide simulation results to illustrate the performance of detecting the moving target with multiple moving radar platforms. As shown in Fig. 4, there are $M = 2$ TXs and $N = 2$ RXs, and each TX or RX has $P_m = Q_n = 4$ antennas $(m = 1, 2; n = 1, 2)$. The positions and antenna angles of TXs and RXs are shown in Table I, where the antenna angle is defined as the angle between the antenna array and x-axis in Fig. 4. The carrier frequency is $f_c = 1$ GHz, the velocity of light is $c = 3 \times 10^8$ m/s, the waveform length is $\lambda = 0.3$ m, and the antennas spacing is $d_T = \frac{\lambda}{2} = 0.15$ m. The pulse number is $K = 8$, the PRI is $T_p = 0.25$ ms, the pulse repetition frequency (PRF) is $\frac{1}{T_p} = 4$ KHz, and the signal length is $L = 16$. There is $C_{m,n} = 3$ $(m = 1, 2; n = 1, 2)$ clutter around target for each TX-RX pair, the scattering coefficients of target and clutter are $\alpha_{m,n} = \beta_{m,n,c} = 1$. The signal-to-clutter ratio (SCR) of the echo waveform is defined as

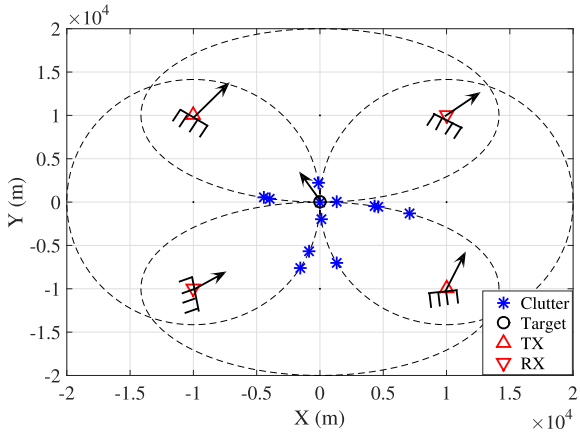

Fig. 4. The simulated moving target and MIMO radar platforms.

TABLE I
Target and Radar Parameters

	Position (m)	Velocity (m/s)	Antenna angle
TX1	$\boldsymbol{p}_{T,1} = (-10^4, 10^4)^T$	$\boldsymbol{v}_{T,1} = (43.31, 47.03)^T$	329.77°
TX2	$\boldsymbol{p}_{T,2} = (10^4, -10^4)^T$	$\boldsymbol{v}_{T,2} = (21.35, 43.70)^T$	190.05°
RX1	$\boldsymbol{p}_{R,1} = (10^4, 10^4)^T$	$\boldsymbol{v}_{R,1} = (32.94, 31.98)^T$	321.88°
RX2	$\boldsymbol{p}_{R,2} = (-10^4, -10^4)^T$	$\boldsymbol{v}_{R,2} = (34.51, 38.75)^T$	96.71°

$$\mathrm{SCR} \triangleq \frac{\mathbb{E}\{\boldsymbol{y}^H \boldsymbol{y}\}}{\mathbb{E}\{\boldsymbol{z}^H \boldsymbol{z}\}}, \tag{55}$$

and SCNR is defined as

$$\mathrm{SCNR} \triangleq \frac{\mathbb{E}\{\boldsymbol{y}^H \boldsymbol{y}\}}{\mathbb{E}\{\boldsymbol{z}^H \boldsymbol{z}\} + \mathbb{E}\{\boldsymbol{n}^H \boldsymbol{n}\}}. \tag{56}$$

Since the noise can be greatly reduced by the accumulation in the detection, the detection performance is mostly affected by the clutter. In our simulations, we use the SCNR setting of -28 dB and -31 dB. The strong clutter scatterers are sparse in the radar detection area, but the low-level bald earth clutter scatterers [55] are not sparse and there are multiple low-level clutter scatterers in each resolution cell. The power ratio between the strong sparse clutter and the bald earth clutter is 10 dB. In Algorithm 1 to estimate the scattering coefficients and angles of clutter, the angle resolution of the dictionary matrix is $\Delta\zeta = 2$, and the detection area $\boldsymbol{\zeta}$ is 100 around the target. For example, for TX1-RX1 pair, the target angle is $\theta_{1,1} = 90$ and the detection area $\boldsymbol{\zeta}$ is from 40 to 140. To show the average target detection performance, 10^4 simulations are preformed. The target velocity $\boldsymbol{v} = [v_x, v_y]^T$ is chosen uniformly $(\{v_x, v_y\} \sim \mathrm{unif}\,[0, 100]$

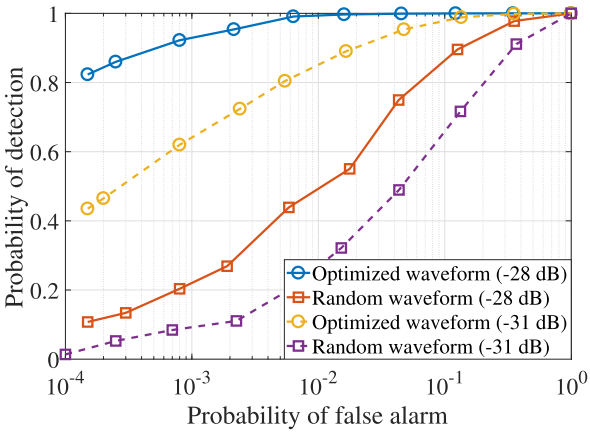

Fig. 5. ROC curves with optimized waveforms (perfect target and clutter information).

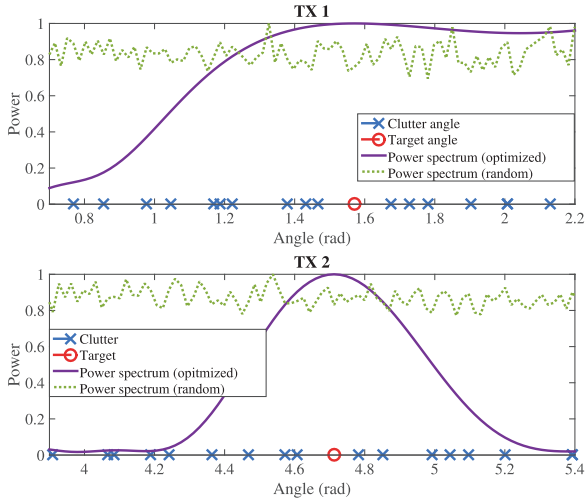

Fig. 6. The power spectrum of optimized waveforms.

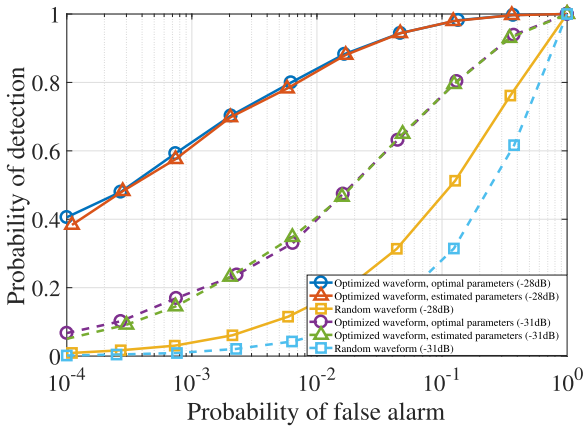

Fig. 7. ROC curves with optimized waveforms (estimated target and clutter parameters).

m/s), and the clutter are uniformly distributed around the target in each simulation.

A. Effect of Waveform Optimization With Perfect Parameters of Target and Clutter

First, with the perfect Parameter information of target and clutter, we optimize the transmitted waveform based on the method proposed in Section V, and the receiver operating characteristic (ROC) curves are shown in Fig. 5. The curves for random waveforms are obtained by averaging the ROC curves of 10^4 Gaussian random waveforms. Since the parameters are known, the likelihood ratio test (instead of GLRT) is used, and the ROC performance improvement due to waveform optimization is clearly shown in Fig. 5. By optimizing the transmitted waveforms, the target detection performance can be significantly enhanced. However, in practice, the parameters of target and clutter are unknown, and they are estimated using Algorithm 1 and Algorithm 2 in the following simulations. The estimated parameters are used in both waveform optimization and in GLRT.

B. Effect of Waveform Optimization With Estimated Parameters of Target and Clutter

By optimizing the transmitted waveform, the transmit beampattern forms nulls at the clutter directions, and a peak at the target direction. Therefore, the SCNR of the received signal can be increased. In Fig. 6, the transmit beampattern of the optimized waveform and the beampattern of the Gaussian random waveform are plotted against the angle of the surveillance area. Two TX platforms denoted as TX 1 and TX 2 are used to transmit the waveforms, and the waveform is individually optimized at each platform. The optimized waveforms at both TX platforms has large power gain at the target direction, while having small power gain at the clutter direction, as shown in Fig. 6. However, the random waveform has almost the same power gain over all the angle, and cannot improve the SCNR of the received signal. As a result, the better detection performance can be achieved by the optimized waveform.

In Fig. 7, the clutter positions, target velocity and scattering coefficients are estimated by Algorithm 1 and Algorithm 2. Then, the GLRT is performed based on (25). In this figure, three types of waveforms are compared including the random waveform, the optimized waveform with the perfect parameter information of target and clutter, and the optimized waveform with the estimated parameters of target and clutter. By optimizing the transmitted waveform, the target detection performance can be significantly improved. Additionally, the optimized waveforms with the estimated parameters of target and clutter have almost the same performance as those with perfect information, where the estimated parameters are obtained from the echo waveforms of the random transmitted waveforms.

C. Comparison With the Distributed MIMO Radar

In Fig. 8, we compare the ROC performance of the proposed system with that of the distributed MIMO radar [3]. In these simulations, the random waveforms are transmitted first, and both Algorithm 1 and Algorithm 2 are used for the rough estimation of the target and clutter parameters. Then, the transmitted waveforms are optimized according to the estimated parameters, and the GLRT is used for detection based on the optimized waveforms. The distributed MIMO radar has the same

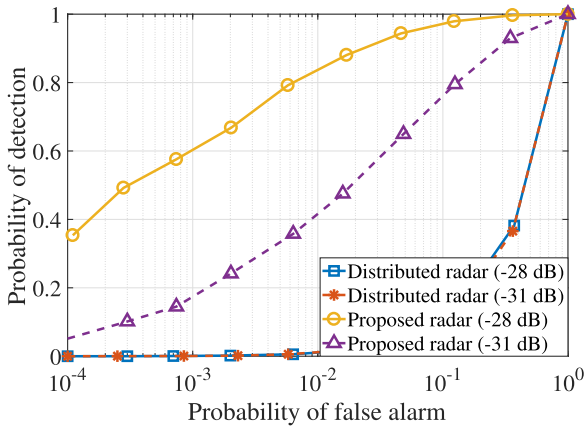

Fig. 8. ROC comparison of the proposed and distributed MIMO radar.

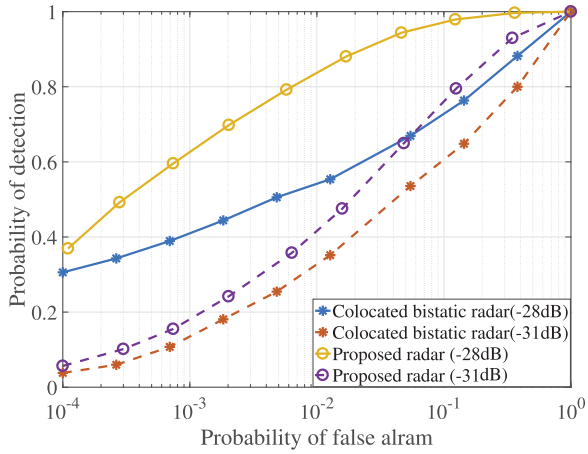

Fig. 9. ROC comparison of the proposed and colocated bistatic MIMO radar.

system parameters with the proposed radar system, but there is only one antenna at each moving platform ($P_m = Q_n = 1$, $m = 1, 2$; $n = 1, 2$). Hence there is no freedom to optimize the transmitted waveforms and to improve the SCNR, and hence constant waveforms with full power are transmitted in the distributed MIMO radar. It is seen that, for both SCNR $= -28$ dB and SCNR $= -31$ dB, the proposed radar system achieves better target detection performance than the distributed MIMO radar system. Additionally, the ROC performance is improved more significantly by increasing the SCNR in the proposed radar system than that in the distributed MIMO radar system.

D. Comparison With the Colocated Bistatic MIMO Radar

In Fig. 9, we compare the ROC performance of the proposed radar system with that of the colocated bistatic MIMO radar, which corresponds to $M = N = 1$ in the proposed radar system. In these simulations, the parameters of clutter and target are estimated according to the random waveforms. Then, the transmitted waveforms are also optimized based on the estimated parameters, and finally the GLRT is adopted to detect the target. Since the positions, velocities and antenna angles of radar platforms affect the target detection performance, all these parameters are the same for both the proposed radar and

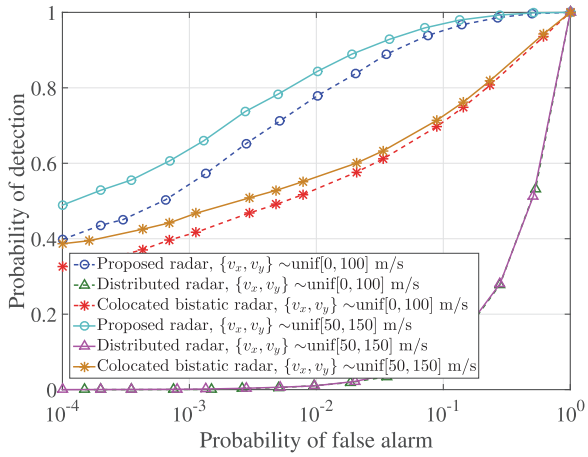

Fig. 10. ROC curves with different target velocities.

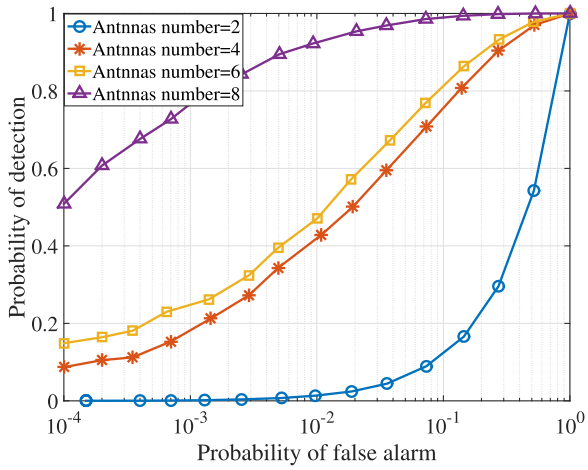

Fig. 11. ROC curves with different number of antennas.

the colocated bistatic MIMO radar. The transmitted waveforms are optimized in both radar systems. Since more platform diversity can be provided in the proposed radar system, it is seen that a better ROC performance is achieved compared with the colocated bistatic MIMO radar.

E. Effects of Various Parameters

1) Target Velocity: Since the target is distinguished from the clutter by the different velocity, we show the velocity effect in Fig. 10. The target velocity is set randomly from $\{v_x, v_y\} \sim$ unif $[0, 100]$ m/s and $\{v_x, v_y\} \sim$ unif $[50, 150]$ m/s. Increasing the target velocity can improve the target detection performance in both the proposed and colocated radars, but not so in the distributed MIMO radar. For a given target velocity, a better ROC performance is achieved by the proposed radar system than both the distributed and colocated MIMO radars. Additionally, more significant ROC improvement can be achieved by increasing the target velocity in the proposed radar system.

2) Antenna Number: In Fig. 11, the effect of antenna number is demonstrated, where $P_m = Q_n \in \{2, 4, 6, 8\}$, $(m = 1, 2;$ $n = 1, 2)$. Since increasing the antenna number can improve the degree of freedom in waveform optimization, better ROC per-

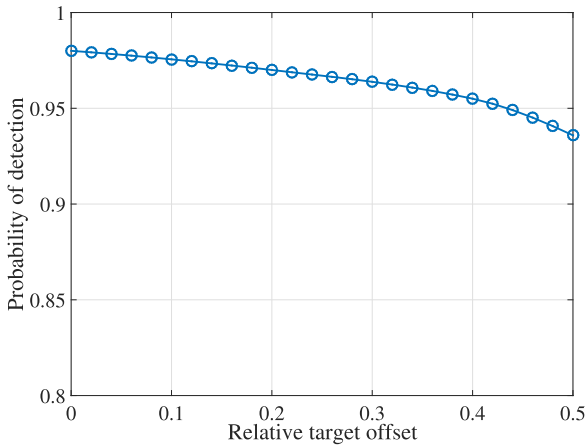

Fig. 12. Detection performance with target offsets and $P_{FA} = 0.1$.

formance can also be achieved. Therefore, more antennas are preferred in the proposed radar system.

3) Target Offset: In Fig. 12, the sensitivity of our algorithm is given, where the detection probability of the proposed algorithm is plotted against the relative range offset of the target. Here the relative offset is defined as the fraction of target offset and the size of range resolution cell. As can be seen from the figure, as the relative offset increases, the detection probability will decrease slightly. The decrease in the detection performance is within 5%. Hence, it is reasonable to conclude that the proposed method of target detection is not sensitive to a slight target offset.

VII. Conclusion

We have proposed a novel radar system for detecting moving target by multiple moving platforms, where colocated MIMO antennas are used in each platform. To exploit the geographical sparsity of clutter, the CS-based model has been employed, and a novel two-step OMP algorithm has been proposed to solve the clutter off-grid problem. Then, the moving target can be detected by the GLRT detector in the fusion center. To further improve the target detection performance, a novel waveform optimization technique has been proposed to maximize the SCNR of echo waveform in each moving transmitter platform. Simulation results demonstrate the advantages of the proposed radar system in detecting the moving target over the existing distributed and colocated MIMO radars, and both the waveform optimization and the proposed reconstruction algorithm can further improve the detection performance. Further works will focus on the detection problem with multiple moving targets in the proposed radar system.

Appendix

In Section II, the echo waveform as a function of both delay and Doppler frequency is given. In this appendix, we give the expresses of delay and Doppler frequency based on the geometrical relationship between the target and radar platforms.

The delay from the (m,p)-th TX antenna to the (n,q)-th RX antennas is [57]

$$\tau_{(m,p),(n,q)}(\theta_{m,n}) = \frac{d_T}{c}\left[(p-1)\cos\theta_{T,m} + (q-1)\cos\theta_{R,n}\right]. \tag{57}$$

As shown in Fig. 2, the target view angles from TX and RX can be denoted as $\theta_{T,m}$ and $\theta_{R,n}$ respectively, which can be obtained by the geometrical relationship of ellipse [37], [58] as (58) and (59) at the bottom of this page, where $\eta_{1,m,n} \triangleq \frac{1}{2}\left(\left\|\boldsymbol{p}-\boldsymbol{p}_{T,m}\right\|_2 + \left\|\boldsymbol{p}-\boldsymbol{p}_{R,n}\right\|_2\right)$ and $\eta_{2,m,n} \triangleq \sqrt{\eta_{1,m,n}^2 - \frac{1}{4}\left\|\boldsymbol{p}_{T,m}-\boldsymbol{p}_{R,n}\right\|_2^2}$ denote respectively the major and minor axes of the ellipse formed by the m-th TX and n-th RX which are assumed constants during the K pulses of observations. The parameter $\theta'_{m,n}$ has the following relationship with target angle $\theta_{m,n}$ [37]

$$\theta_{m,n} = \arccos\left(\frac{\eta_{1,m,n}\cos\theta'_{m,n}}{\sqrt{\left(\eta_{1,m,n}\cos\theta'_{m,n}\right)^2 + \left(\eta_{2,m,n}\sin\theta'_{m,n}\right)^2}}\right). \tag{60}$$

Therefore, for the given TX-RX pair, the delay $\tau_{(m,p),(n,q)}(\theta_{m,n})$ is a function of target angle $\theta_{m,n}$.

The Doppler frequency $f_{d,m,n}(\theta_{m,n},\boldsymbol{v})$ can be obtained by[3]

$$f_{d,m,n}(\theta_{m,n},\boldsymbol{v}) = \frac{f_c}{c}\left[\boldsymbol{d}_{T,m}^T(\theta_{m,n})(\boldsymbol{v}_{T,m}-\boldsymbol{v}) + \boldsymbol{d}_{R,n}^T(\theta_{m,n})(\boldsymbol{v}_{R,n}-\boldsymbol{v})\right], \tag{61}$$

where $\boldsymbol{d}_{T,m}(\theta_{m,n}) \triangleq \frac{\boldsymbol{p}-\boldsymbol{p}_{T,m}}{\left\|\boldsymbol{p}-\boldsymbol{p}_{T,m}\right\|_2}$ and $\boldsymbol{d}_{R,n}(\theta_{m,n}) \triangleq \frac{\boldsymbol{p}-\boldsymbol{p}_{R,n}}{\left\|\boldsymbol{p}-\boldsymbol{p}_{R,n}\right\|_2}$ denote respectively the directions from the m-th TX and the n-th RX to the target.

Additionally, from (1) to (2), the continuous-time signal $s_{m,p}(t)$ is sampled by a sufficiently high sampling frequency, and a discrete-time vector $\boldsymbol{s}_{m,p}$ is obtained. Then, during the k-th pulse, the signal with only relative delay $\tau_{(m,p),(n,q)}(\theta_{m,n})$

$$\theta_{T,m} = \arccos\left(\frac{\eta_{1,m,n}\cos\theta'_{m,n} + \sqrt{\eta_{1,m,n}^2 - \eta_{2,m,n}^2}}{\sqrt{\left(\eta_{2,m,n}\sin\theta'_{m,n}\right)^2 + \left(\eta_{1,m,n}\cos\theta'_{m,n} + \sqrt{\eta_{1,m,n}^2 - \eta_{2,m,n}^2}\right)^2}}\right), \tag{58}$$

$$\theta_{R,n} = \arccos\left(\frac{\eta_{1,m,n}\cos\theta'_{m,n} - \sqrt{\eta_{1,m,n}^2 - \eta_{2,m,n}^2}}{\sqrt{\left(\eta_{2,m,n}\sin\theta'_{m,n}\right)^2 + \left(\eta_{1,m,n}\cos\theta'_{m,n} - \sqrt{\eta_{1,m,n}^2 - \eta_{2,m,n}^2}\right)^2}}\right), \tag{59}$$

and Doppler frequency $f_{d,m,n}(\theta_{m,n}, \boldsymbol{v})$ can be represented as $\boldsymbol{s}_{m,p}e^{-j2\pi f_c \tau_{(m,p),(n,q)}(\theta_{m,n})}$ and $\boldsymbol{s}_{m,p}e^{-j2\pi k T_p f_{d,m,n}(\theta_{m,n},\boldsymbol{v})}$, respectively. Therefore, the discrete-time model in (2) can be obtained from the signal with both delay and Doppler frequency.

REFERENCES

[1] E. Fishler, A. Haimovich, R. S. Blum, L. J. Cimini, D. Chizhik, and R. A. Valenzuela, "Spatial diversity in radars-models and detection performance," *IEEE Trans. Signal Process.*, vol. 54, no. 3, pp. 823–838, Mar. 2006.

[2] E. Fishler, A. Haimovich, R. Blum, D. Chizhik, L. Cimini, and R. Valenzuela, "MIMO radar: An idea whose time has come," in *Proc. IEEE Radar Conf.*, Apr. 2004, pp. 71–78.

[3] H. Li, Z. Wang, J. Liu, and B. Himed, "Moving target detection in distributed MIMO radar on moving platforms," *IEEE J. Sel. Top. Signal Process.*, vol. 9, no. 8, pp. 1524–1535, Dec. 2015.

[4] Q. He, N. H. Lehmann, R. S. Blum, and A. M. Haimovich, "MIMO radar moving target detection in homogeneous clutter," *IEEE Trans. Aerosp. Electron. Syst.*, vol. 46, no. 3, pp. 1290–1301, Jul. 2010.

[5] W. L. Melvin, "Space-time adaptive radar performance in heterogeneous clutter," *IEEE Trans. Aerosp. Electron. Syst.*, vol. 36, no. 2, pp. 621–633, Apr. 2000.

[6] R. Klemm, *Principles of Space-Time Adaptive Processing*. London, U.K.: Inst. Eng. Technol., 2006.

[7] P. Wang, H. Li, and B. Himed, "Moving target detection using distributed MIMO radar in clutter with nonhomogeneous power," *IEEE Trans. Signal Process.*, vol. 59, no. 10, pp. 4809–4820, Jun. 2011.

[8] J. Liu, Z.-J. Zhang, Y. Cao, and S. Yang, "A closed-form expression for false alarm rate of adaptive MIMO-GLRT detector with distributed MIMO radar," *Signal Process.*, vol. 93, no. 9, pp. 2771–2776, Sep. 2013.

[9] N. Li, G. Cui, L. Kong, and Q. H. Liu, "Moving target detection for polarimetric multiple-input multiple-output radar in Gaussian clutter," *IET Radar, Sonar Navig.*, vol. 9, no. 3, pp. 285–298, Mar. 2015.

[10] N. Li, G. Cui, L. Kong, and X. Yang, "MIMO radar moving target detection against compound-gaussian clutter," *Circuits, Syst. Signal Process.*, vol. 33, no. 6, pp. 1819–1839, Jun. 2014.

[11] C. Y. Chong, F. Pascal, J. Ovarlez, and M. Lesturgie, "MIMO radar detection in non-gaussian and heterogeneous clutter," *IEEE J. Sel. Top. Signal Process.*, vol. 4, no. 1, pp. 115–126, Feb. 2010.

[12] M. Hurtado and A. Nehorai, "Polarimetric detection of targets in Heavy inhomogeneous clutter," *IEEE Trans. Signal Process.*, vol. 56, no. 4, pp. 1349–1361, Apr. 2008.

[13] T. Zhang, G. Cui, L. Kong, and X. Yang, "Adaptive bayesian detection using MIMO radar in spatially heterogeneous clutter," *IEEE Signal Process. Lett.*, vol. 20, no. 6, pp. 547–550, Mar. 2013.

[14] P. Wang, H. Li, and B. Himed, "A parametric moving target detector for distributied MIMO radar in non-homogeneous environment," *IEEE Trans. Signal Process.*, vol. 61, no. 9, pp. 2282–2294, May 2013.

[15] S. Y. Chao and B. X. Chen, "FDGLRT detector of MIMO radar in non-homogeneous clutter," *Electron. Lett.*, vol. 47, no. 6, pp. 403–404, Mar. 2011.

[16] W. Liu, Y. Wang, J. Liu, W. Xie, H. Chen, and W. Gu, "Adaptive detection without training data in colocated MIMO radar," *IEEE Trans. Aerosp. Electron. Syst.*, vol. 51, no. 3, pp. 2469–2479, Jul. 2015.

[17] L. Guo, H. Deng, B. Himed, T. Ma, and Z. Geng, "Waveform optimization for transmit beamforming with MIMO radar antenna arrays," *IEEE Trans. Antennas Propag.*, vol. 63, no. 2, pp. 543–552, Dec. 2015.

[18] D. R. Fuhrmann and G. S. Antonio, "Transmit beamforming for MIMO radar systems using signal cross-correlation," *IEEE Trans. Aerosp. Electron. Syst.*, vol. 44, no. 1, pp. 171–186, Jan. 2008.

[19] P. Stoica, L. Jian, and Z. Xumin, "Waveform synthesis for diversity-based transmit beampattern design," *IEEE Trans. Signal Process.*, vol. 56, no. 6, pp. 2593–2598, Jun. 2008.

[20] J. Liu, H. Li, and B. Himed, "Joint optimization of transmit and receive beamforming in active arrays," *IEEE Signal Process. Lett.*, vol. 21, no. 1, pp. 39–42, Nov. 2014.

[21] H. Xu, J. Wang, J. Yuan, and X. Shan, "Colocated MIMO radar transmit beamspace design for randomly present target detection," *IEEE Signal Process. Lett.*, vol. 22, no. 7, pp. 828–832, Nov. 2015.

[22] A. Leshem, O. Naparstek, and A. Nehorai, "Information theoretic adaptive radar waveform design for multiple extended targets," *IEEE J. Sel. Top. Signal Process.*, vol. 1, no. 1, pp. 42–55, Jun. 2007.

[23] B. Tang, J. Tang, and Y. Peng, "Waveform optimization for MIMO radar in colored noise: Further results for estimation-oriented criteria," *IEEE Trans. Signal Process.*, vol. 60, no. 3, pp. 1517–1522, Nov. 2012.

[24] T. Naghibi and F. Behnia, "MIMO radar waveform design in the presence of clutter," *IEEE Trans. Aerosp. Electron. Syst.*, vol. 47, no. 2, pp. 770–781, Apr. 2011.

[25] G. Cui, H. Li, and M. Rangaswamy, "MIMO radar waveform design with constant modulus and similarity constraints," *IEEE Trans. Signal Process.*, vol. 62, no. 2, pp. 343–353, Oct. 2014.

[26] C.-Y. Chen and P. P. Vaidyanathan, "MIMO radar waveform optimization with prior information of the extended target and clutter," *IEEE Trans. Signal Process.*, vol. 57, no. 9, pp. 3533–3544, Apr. 2009.

[27] Y. Yang, R. S. Blum, Z. He, and D. R. Fuhrmann, "MIMO radar waveform design via alternating projection," *IEEE Trans. Signal Process.*, vol. 58, no. 3, pp. 1440–1445, Sep. 2010.

[28] C. Chun-Yang and P. P. Vaidyanathan, "MIMO radar ambiguity properties and optimization using frequency-hopping waveforms," *IEEE Trans. Signal Process.*, vol. 56, no. 12, pp. 5926–5936, Aug. 2008.

[29] C. Gao, K. C. Teh, and A. Liu, "Orthogonal frequency diversity waveform with range-Doppler optimization for MIMO radar," *IEEE Signal Process. Lett.*, vol. 21, no. 10, pp. 1201–1205, Jun. 2014.

[30] B. Jiu, H. Liu, X. Wang, L. Zhang, Y. Wang, and B. Chen, "Knowledge-based spatial-temporal hierarchical MIMO radar waveform design method for target detection in heterogeneous clutter zone," *IEEE Trans. Signal Process.*, vol. 63, no. 3, pp. 543–554, Oct. 2015.

[31] M. Hurtado and A. Nehorai, "Polarization diversity for detecting targets in inhomogeneous clutter," in *Proc. Int. Waveform Diversity Des. Conf.*, Pisa, Italy, 2007, pp. 382–386.

[32] K. Hayashi, M. Nagahara, and T. Tanaka, "A user's guide to compressed sensing for communications systems," *IEICE Trans. Commun.*, vol. E96.B, no. 3, pp. 685–712, Mar. 2013.

[33] Z. Tan and A. Nehorai, "Sparse direction of arrival estimation using co-prime arrays with off-grid targets," *IEEE Signal Process. Lett.*, vol. 21, no. 1, pp. 26–29, Jan. 2014.

[34] A. M. Haimovich, R. S. Blum, and L. J. Cimini, "MIMO radar with widely separated antennas," *IEEE Signal Process. Mag.*, vol. 25, no. 1, pp. 116–129, Dec. 2008.

[35] J. Li and P. Stoica, "MIMO radar with colocated antennas," *IEEE Signal Process. Mag.*, vol. 24, no. 5, pp. 106–114, Sep. 2007.

[36] M. Davis, G. Showman, and A. Lanterman, "Coherent MIMO radar: The phased array and orthogonal waveforms," *IEEE Aerosp. Electron. Syst. Mag.*, vol. 29, no. 8, pp. 76–91, Aug. 2014.

[37] N. J. Willis and H. D. Griffiths, *Advances in Bistatic Radar*. Rayleigh, NC, USA: SciTech Publishing, Inc., 2007.

[38] J. Zhang, H. Wang, and X. Zhu, "Adaptive waveform design for separated transmit/receive ULA-MIMO radar," *IEEE Trans. Signal Process.*, vol. 58, no. 9, pp. 4936–4942, Jun. 2010.

[39] A. Tajer, G. Jajamovich, X. Wang, and G. Moustakides, "Optimal joint target detection and parameter estimation by MIMO radar," *IEEE J. Sel. Top. Signal Process.*, vol. 4, no. 1, pp. 127–145, Feb. 2010.

[40] G. Moustakides, G. Jajamovich, A. Tajer, and X. Wang, "Joint detection and estimation: Optimum tests and applications," *IEEE Trans. Inf. Theory*, vol. 58, no. 7, pp. 4215–4229, Jul. 2012.

[41] G. Jajamovich, M. Lops, and X. Wang, "Space-time coding for MIMO radar detection and ranging," *IEEE Trans. Signal Process.*, vol. 58, no. 12, pp. 6195–6206, Dec. 2010.

[42] R. Boyer, "Performance bounds and angular resolution limit for the moving colocated MIMO radar," *IEEE Trans. Signal Process.*, vol. 59, no. 4, pp. 1539–1552, Apr. 2011.

[43] J. B. Billingsley, A. Farina, F. Gini, M. V. Greco, and L. Verrazzani, "Statistical analyses of measured radar ground clutter data," *IEEE Trans. Aerosp. Electron. Syst.*, vol. 35, no. 2, pp. 579–593, Apr. 1999.

[44] J. Ward, *Space-Time Adaptive Processing for Airborn Radar*. Lexington, MA, USA: Massachusetts Inst. Technol. Lincoln Lab., 1994.

[45] S. M. Kay, *Fundamentals of Statistical Signal Processing, Volume II: Detection Theory*. Englewood Cliffs, NJ, USA: Prentice-Hall.

[46] Y. Chi, L. Scharf, A. Pezeshki, and A. Calderbank, "Sensitivity to basis mismatch in compressed sensing," *IEEE Trans. Signal Process.*, vol. 59, no. 5, pp. 2182–2195, May 2011.

[47] Z. Yang, L. Xie, and C. Zhang, "Off-grid direction of arrival estimation using sparse bayesian inference," *IEEE Trans. Signal Process.*, vol. 61, no. 1, pp. 38–43, Jan. 2013.
[48] L. Bai, S. Roy, and M. Rangaswamy, "Compressive radar clutter subspace estimation using dictionary learning," in *Proc. IEEE Radar Conf.*, Ottawa, ON, Canada, Apr. 2013, pp. 1–6.
[49] X. Zhan, R. Zhang, D. Yin, and C. Huo, "SAR image compression using multiscale dictionary learning and sparse representation," *IEEE Geosci. Remote Sens. Lett.*, vol. 10, no. 5, pp. 1090–1094, Jan. 2013.
[50] S. Becker, J. Bobin, and E. Candes, "Nesta a fast and accurate first order method for sparse recovery," *SIAM J. Imag. Sci.*, vol. 4, pp. 1–39, 2011.
[51] S. Boyd and L. Vandenberghe, *Convex Optimization*. Cambridge, U.K.: Cambridge Univ. Press, 2004.
[52] A. Charnes and W. W. Cooper, "Programming with linear fractional functionals," *Naval Res. Logist. Quart.*, vol. 9, no. 3–4, pp. 181–186, 1962.
[53] Z. Q. Luo, W. K. Ma, A. M. C. So, Y. Y. Ye, and S. Z. Zhang, "Semidefinite relaxation of quadratic optimization problems," *IEEE Signal Process. Mag.*, vol. 27, no. 3, pp. 20–34, May 2010.
[54] M. Grant and S. Boyd, "CVX: Matlab software for disciplined convex programming, version 2.1," Mar. 2014. [Online]. Available: http://cvxr.com/cvx
[55] P. Gamba and B. Houshmand, "Comparison of C- and X-band InSAR data for 3D characterization of an urban area," *IEEE Aerosp. Electron. Syst. Mag.*, vol. 17, no. 6, pp. 9–15, Jun. 2002.
[56] X. Zhang, F. He, L. Tian, and S. Wang, "Cognitive pedestrian detector: Adapting detector to specific scene by transferring attributes," *Neurocomputing*, vol. 149, pp. 800–810, 2015.
[57] F. K. W. Chan, H. C. So, H. Lei, and H. Long-ting, "Parameter estimation and identifiability in bistatic multiple-input multiple-output radar," *IEEE Trans. Aerosp. Electron. Syst.*, vol. 51, no. 3, pp. 2047–2056, Jul. 2015.
[58] J. Wu, T. Wang, L. Zhang, and Z. Bao, "Range-dependent clutter suppression for airborne sidelooking radar using MIMO technique," *IEEE Trans. Aerosp. Electron. Syst.*, vol. 48, no. 4, pp. 3647–3654, Oct. 2012.

Peng Chen (M'17) was born in Jiangsu, China, in 1989. He received the B.E. and Ph.D. degrees both in information and communication engineering from the School of Information Science and Engineering, Southeast University, Nanjing, China, in 2011 and 2017, respectively.

He joined the teaching staff of the State Key Laboratory of Millimeter Waves, Southeast University, in 2017. His research interests include radar signal processing and millimeter wave communication.

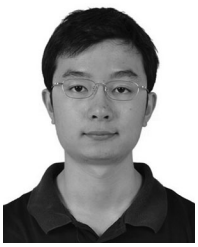

Le Zheng (M'17) was born in Hebei, China, in 1987. He received the B.S. degree in communication engineering from Northwestern Polytechnical University, Xi'an, China, in 2009, and the Ph.D. degree in target detection and recognition from the Beijing Institute of Technology, Beijing, China, in 2015. From October 2013 to October 2014, he was a Visiting Scholar in the Electrical Engineering Department, Columbia University, New York, NY, USA, where he is currently a Postdoctoral Researcher. His research interests include the areas of statistical signal processing, high-performance hardware for signal processing, and radar system and data fusion.

Xiaodong Wang (S'98–M'98–SM'04–F'08) received the Ph.D. degree in electrical engineering from Princeton University, Princeton, NJ, USA, in 1998. He is a Professor of Electrical Engineering at Columbia University, New York, NY, USA. Among his publications is a book entitled *Wireless Communication Systems: Advanced Techniques for Signal Reception* (Prentice-Hall, 2003). His research interests include the general areas of computing, signal processing and communications, and has published extensively in these areas. His current research interests include wireless communications, statistical signal processing, and genomic signal processing.

He received the 1999 NSF CAREER Award, the 2001 IEEE Communications Society and Information Theory Society Joint Paper Award, and the 2011 IEEE Communication Society Award for Outstanding Paper on New Communication Topics. He has served as an Associate Editor for the IEEE TRANSACTIONS ON COMMUNICATIONS, the IEEE TRANSACTIONS ON WIRELESS COMMUNICATIONS, the IEEE TRANSACTIONS ON SIGNAL PROCESSING, and the IEEE TRANSACTIONS ON INFORMATION THEORY. He is listed as an ISI Highly cited Author.

Hongbin Li (M'99–SM'08) received the B.S. and M.S. degrees from the University of Electronic Science and Technology of China, Chengdu, China, in 1991 and 1994, respectively, and the Ph.D. degree from the University of Florida, Gainesville, FL, USA, in 1999, all in electrical engineering.

From July 1996 to May 1999, he was a Research Assistant in the Department of Electrical and Computer Engineering, University of Florida. Since July 1999, he has been with the Department of Electrical and Computer Engineering, Stevens Institute of Technology, Hoboken, NJ, USA, where he became a Professor in 2010. He was a Summer Visiting Faculty Member at the Air Force Research Laboratory in the summers of 2003, 2004, and 2009. His general research interests include statistical signal processing, wireless communications, and radars.

He received the IEEE Jack Neubauer Memorial Award in 2013 from the IEEE Vehicular Technology Soceity, the Outstanding Paper Award from the IEEE AFICON Conference in 2011, the Harvey N. Davis Teaching Award in 2003 and the Jess H. Davis Memorial Award for excellence in research in 2001 from Stevens Institute of Technology, and the Sigma Xi Graduate Research Award from the University of Florida in 1999. He has been a member of the IEEE SPS Signal Processing Theory and Methods Technical Committee (TC) and the IEEE SPS Sensor Array and Multichannel TC, an Associate Editor for *Signal Processing* (Elsevier), IEEE TRANSACTIONS ON SIGNAL PROCESSING, IEEE SIGNAL PROCESSING LETTERS, and IEEE TRANSACTIONS ON WIRELESS COMMUNICATIONS, as well as a Guest Editor for IEEE JOURNAL OF SELECTED TOPICS IN SIGNAL PROCESSING and *EURASIP Journal on Applied Signal Processing*. He has been involved in various conference organization activities, including serving as a General Co-Chair for the 7th IEEE Sensor Array and Multichannel Signal Processing (SAM) Workshop, Hoboken, NJ, June 17–20, 2012. He is a member of Tau Beta Pi and Phi Kappa Phi.

Lenan Wu received the M.S. degree in the electronics communication system from Nanjing University of Aeronautics and Astronautics, Nanjing, China, in 1987, and the Ph.D. degree in signal and information processing from Southeast University, Nanjing, in 1997.

Since 1997, he has been with Southeast University, where he is a Professor, and the Director of Multimedia Technical Research Institute. He is the author or coauthor of more than 400 technical papers and 11 textbooks, and is the holder of 20 Chinese patents and 1 International patent. His research interests include multimedia information systems and communication signal processing.